A high resolution, multi-proxy approach to reconstructing Arabian Sea Oxygen Minimum Zone dynamics

Master thesis Jasper van Bruchem
Faculty of Geosciences, Utrecht University
Supervisors: Dr. Karoliina Koho & Dr. Gert-Jan Reichart
20-12-2012

Abstract
A new deep-sea core from the base of the Arabian Sea Oxygen Minimum Zone (OMZ) spanning the last glacial (75-10 ka) has been analyzed for changes in OMZ intensity. Processes maintaining the Arabian Sea OMZ are surface productivity, stratification of the water mass and advection of oxygen poor deep waters. Productivity is controlled by the strength of the Atlantic Meridional Overturning Circulation (AMOC) and the SW and NE summer and winter monsoons. Minimal OMZ conditions are reconstructed from pteropod and *Globorotalia* abundance records which reflect the CO_3^{2-} saturation state of the bottom waters and the depth of convectional overturning of the surface waters, respectively. The three periods of minimal OMZ intensity which are found in the record lag precession maxima by ~7,000 years. A similar lag has been found for minimum AMOC strength. Thus, we conclude Arabian Sea OMZ variability is mainly driven by changes in the AMOC rather than the monsoons. Comparing the PASOM 3 bromine and C_{org} record with similar records from Murray Ridge stations spanning water depths ranging from 565-2387 m reveals that individual minima and maxima can be correlated in great detail. Shallow stations show sharp minima and maxima while records from deeper stations are much smoother. The PASOM 3 core shows a transition between these two types of records, reflecting the close proximity of the core site to the lower OMZ boundary. Due to the absence of benthic foraminiferal data we do not know whether the OMZ boundary dropped to below the core site at 1172 m depth during the last glacial. A high resolution study has been conducted for the period around Heinrich event 4 (~46-38 ka). Micropaleontological and geochemical proxies are used to reconstruct OMZ variability in this interval. Results show two periods of well oxygenated deep waters (~44-43 & ~40.5-39 ka), occurring during stadial 11 and Heinrich event 4. The composition of the benthic assemblage shows that the base of the OMZ never dropped below the core site at 1172 m during the studied period. Deep overturning of the surface waters, reduced productivity and advection of oxygen-rich Indian Central Water related to the weakening of the AMOC are induced to explain the weakening of the OMZ during H4.

Contents

1. Introduction

Oxygen Minimum Zones (OMZs) are oxygen-deficient water masses at intermediate depths in the world's oceans. The largest OMZs occur in the Arabian Sea and off the west coasts of Africa and Middle and South America. High surface water primary productivities and reduced deep-water ventilation combine to deplete oxygen at intermediate depths (Emerson & Hedges, 2008; Paulmier & Ruiz-Pino, 2009). This depletion is related to oxic degradation of organic matter below the picnocline. Despite the fact that they occupy only a small portion of the world's oceans, OMZ regions play a large role in regulating global climate and more specifically the global nitrogen and carbon cycles (Altabet et al., 2002). In oxygen-deficient settings, nitrate is used as an oxidizing agent by denitrifying bacteria in the remineralization process. This reaction produces, among others, atmospheric nitrogen (N_2), thus removing bioavailable nitrogen from the ocean. Another byproduct of denitrification is N_2O, which is a powerful greenhouse gas. It is estimated that ~50% of all N_2O produced in the world's oceans originates from OMZs (Paulmier & Ruiz-Pino, 2009). In addition, primary producers living at the sea surface fix atmospheric carbon dioxide (CO_2). The high export productivity and preservation of organic carbon in sediments located in OMZs (Paropkari et al., 1992; de Lange et al., 1992; Schulte et al., 1999; Van der Weijden et al., 1999) cause OMZ regions to have a profound effect on global long-time carbon burial (Emerson & Hedges, 2008). Global warming and eutrophication near large river deltas have shown an expansion of OMZs over the last 50 years (Stramma et al., 2008, 2009, 2011). With ongoing anthropogenic emissions of greenhouse gasses, this trend is likely to continue (IPCC, 2007). Since OMZ regions are so important in regulating the marine carbon and nitrogen cycles, it is essential that we understand the complex interactions between OMZs and global climate. This high-resolution multi-proxy study from the lower boundary of one of the largest OMZs in the world provides new insights into functioning of the Arabian Sea OMZ. It allows us to reconstruct how the OMZ changed in response to variations in natural climate over the last 75,000 years. Therefore, this study will further our understanding of the role the Arabian Sea OMZ plays in the regional and global climate. Following Paulmier & Ruiz-Pino (2009), an oxygen concentration of <20 µM or <0.5ml/l is defined in this study as the boundary of the OMZ, since this corresponds to the maximum concentration at which denitrification will still take place. The core of the OMZ is defined as having oxygen concentrations of <2 µM or <0.05 ml/l.

A reconstruction of oceanic and climatic conditions as well as the OMZ variability in the last 75 kyr is made. A number of micropaleontological and geochemical proxies which each reconstruct a specific environmental parameter are used in this respect. In order to study OMZ dynamics during a period of rapid millennial-scale climate changes at a high temporal resolution, this study zooms in on the period surrounding interstadial (IS) 11 and Heinrich event (H) 4 (46-38 ka). In addition to the proxies used in the study of the complete record, reconstructed sea surface temperatures (SSTs) and the organic carbon content of the sediment are used. One of the most powerful tools in the reconstruction of the OMZ during this period is the benthic assemblage. The composition of the benthic foraminiferal assemblage provides direct information about environmental conditions at the sea floor during the studied period.

Questions which are addressed in this study are: how does the OMZ fluctuate spatially and temporally during the last 75,000 years? Can these fluctuations be linked to the orbital parameters and/or oceanic and climatic processes? Can we recognize millennial-scale climate variability in the intensity of the OMZ?

2. Study location

Core PASOM 3 was collected from the Murray Ridge at a depth of 1172 m. The bottom water oxygen concentration at the time of retrieval was approximately 5 µM and the site is thus located

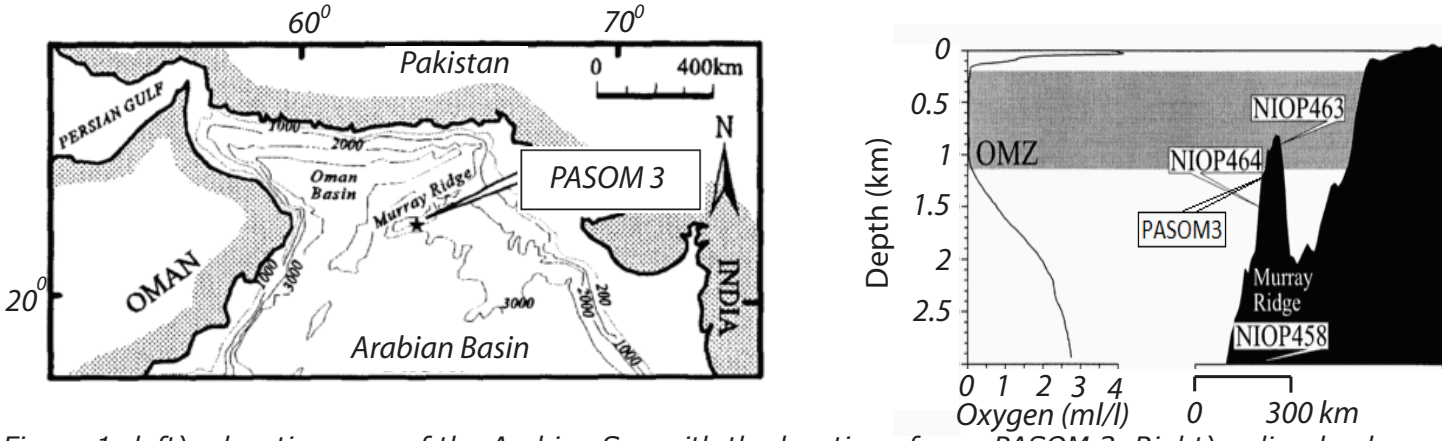

Figure 1; left) a location map of the Arabian Sea with the location of core PASOM 3. Right) a dissolved oxygen profile showing the OMZ which ranges from 200-1200 m depth. Also shown is the Murray Ridge, with the positions of cores NIOP 463, 464 and 458 as well as PASOM 3. Adapted from Reichart et al. (1998) and Den Dulk et al. (2000)

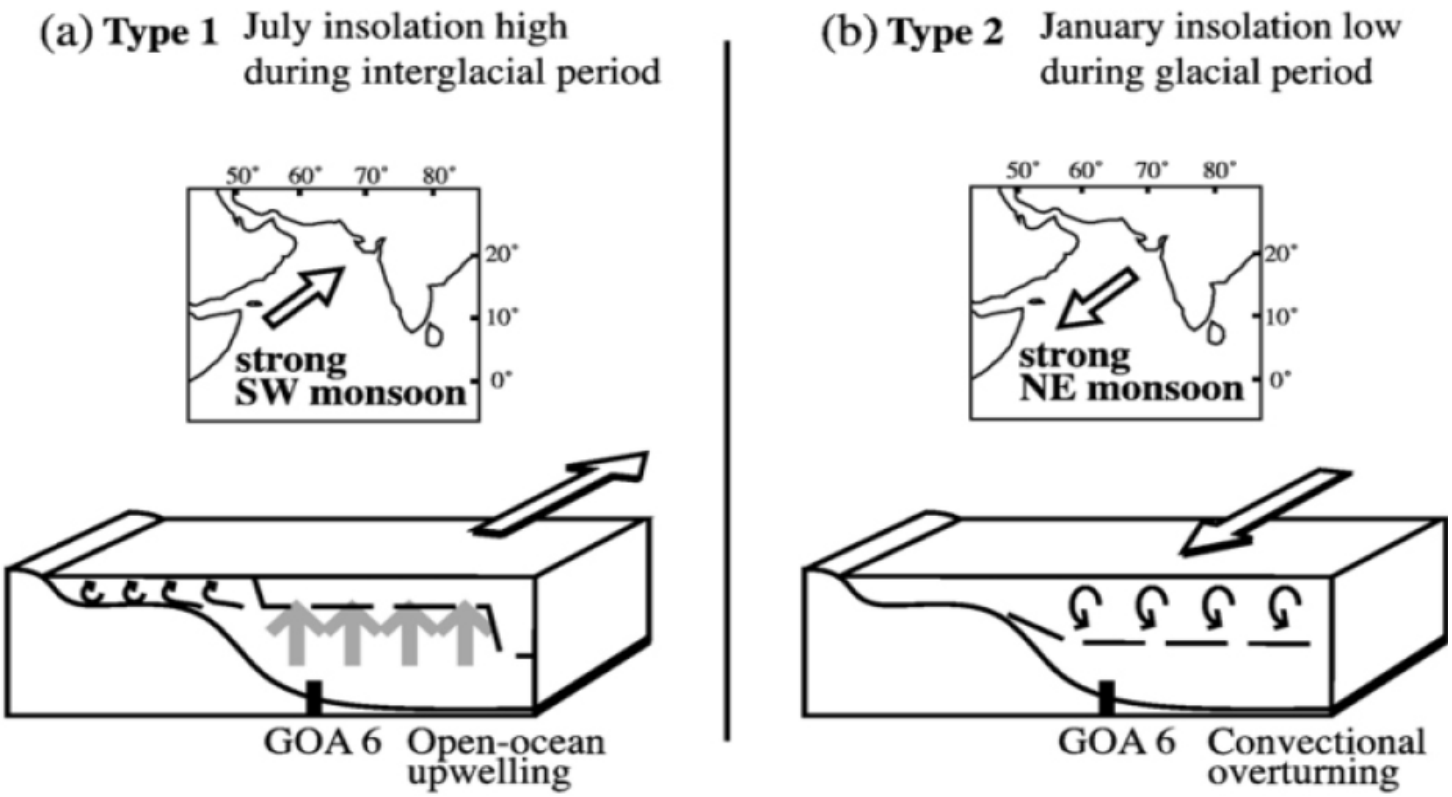

Figure 2; the two scenarios which drive productivity in the Arabian Sea. A) When the SW summer monsoon is intense, strong southwesterly winds drive upwelling of deep, nutrient-rich waters, enhancing productivity. When the winter monsoon is more intense, cooling leads to convectional overturning and erosion of the nutrient-rich deeper waters boosts productivity. Ishikawa et al. (2007)

just above the lower boundary of the OMZ. The proximity of the core site to this boundary provides a unique opportunity to study OMZ dynamics in an open ocean setting. Comparable research has been conducted on cores lying within and below the OMZ at waterdepths of ~900 and ~1500 mbss, respectively (Reichart et al., 1997; Den Dulk et al., 2000; Ziegler et al., 2010). However, no cores from the lower boundary of the OMZ have thus far been analyzed. In addition, the high resolution at which the study window at ~40 ka has been sampled allows us to reconstruct OMZ dynamics at centennial timescales.

3. Hydrographic and climatic setting

3.1 Processes maintaining the Arabian Sea OMZ

The Arabian Sea is characterized by an intense Oxygen Minimum Zone (OMZ) which impinges on the continental shelf at depths of ~150 to ~1200 mbss (fig. 1, Reichart et al., 1997; 1998; 2002; Van der Weijden et al., 1999; Den Dulk et al., 2000; Shailaja et al., 2004; Schumacher et al., 2007; Singh, 2007; Hughes et al., 2008). A complex interplay of a number of processes controls the intensity of the Arabian Sea OMZ. High surface primary productivities lead to depletion of dissolved oxygen at intermediate depths as organic matter sinks through the water column and is subsequently remineralized. The advection of oxygen poor deep water maintains the low oxygen concentrations in the OMZ: the principal source of water at intermediate depths is the Indian Central Water (~1 ml/l, Reichart et al., 1998) which enters the Arabian Sea from the south-west during the Indian summer monsoon (Schulte et al., 1999; Reichart et al., 2004; Pichevin et al., 2007; Böning & Bard, 2009). A third process which controls the OMZ in the Arabian Sea is the overturning depth of the surface waters. High sea surface temperatures combined with the inflow of warm Persian Gulf and Red Sea Water restrict vertical mixing of the oxygen-rich surface waters to the upper 150 m of the water column (Olson et al., 1993; Boyle et al., 1995; Reichart et al. 1998, 2000, 2002; Schult et al., 1999; 2002; Brand & Griffiths, 2009).

Variability in the Arabian Sea OMZ intensity occurs on orbital and millennial timescales. On orbital timescales, global climate fluctuates between glacial and interglacial conditions and on millennial timescales, the climate swings between mild interstadials or Dansgaard-Oescher events (Dansgaard, 1993) and cold stadials. The coldest stadials are related to North Atlantic Heinrich events (Reichart et al., 2004), periods when massive collapse of northern hemisphere ice sheets supplied so much fresh water into the northern Atlantic that deep-water formation was temporarily hampered. These variations in global climate affect the productivity, overturning depth and the oxygen concentrations in the Indian Central Water, thereby influencing the intensity of the OMZ.

3.2 Processes controlling primary productivities in the Arabian Sea

Arabian Sea surface primary productivities are controlled by the Atlantic Meridional Overturning Circulation (AMOC) and the summer and winter monsoons. The strength of the AMOC determines the input of nutrients into the Arabian Sea. A stronger circulation results in the advection of more nutrient-rich deep waters and a subsequent high productivity (Ziegler et al., 2010a). Studies by Schmittner et al. (2005, 2007) have indicated that during periods of minimal deep water advection, export productivities decrease by 30%. A secondary influence is the Indian SW and NE summer and winter monsoons (Reichart et al., 1997, 1998, 2002, 2004, Singh et al., 2011). In northern hemisphere summer, Central Asia heats up and rising air creates a pressure gradient between Tibet and the southern Indian Ocean. As a result, south-westerly winds prevail over the northern Indian Ocean. These winds are funneled into a low-level jet stream known as the Findlater jet (Findlater, 1971; Reichart et al., 1997). Ekman pumping underneath this jet causes upwelling of nutrient-rich, cold waters (fig. 2a) and as a result the Arabian Sea is extremely productive during northern hemisphere summer with annual productivity rates reaching 200-400 g $C/m^2\ yr^{-1}$ (Quasim, 1982; Reichart et al., 1997). In winter, the circulation pattern is reversed as air rises over the relatively warm Indian Ocean and cold north-easterly winds cool the surface water. The subsequent deepening of the thermocline results in enhanced convective overturning of the surface waters. As deeper, nutrient-rich waters are eroded, winter productivities are increased (fig. 2b, Rostek et al., 1997; Reichart et al., 1998, 2002).

A study by Ziegler et al. (2010a) showed that primary productivities in the Arabian Sea are controlled by the strength of the AMOC rather than the intensity of the Indian monsoons. They report a 7,000 year lag between precession minima and productivity maxima. A similar lag exists for maximum strength of the AMOC (Lisiecki et al., 2008; Ziegler et al., 2010a). During periods of maximum precession, northern hemisphere summer insolation is at a minimum (Ruddiman, 2008). Ice sheets grow to a maximum because melting in summer is reduced. In consequence, the climate cools down and the AMOC is reduced. Less input of nutrients into the Arabian Sea subsequently decreases productivity.

The effect of precessional forcing on the Indian summer and winter monsoons is still a subject of debate. Two schools of thought exist: a large number of researchers agree with the model by Kutzbach et al. (1980) in which it is suggested that maximal summer monsoon conditions vary in response to July 21 northern hemisphere (NH) insolation changes. Evidence in favor of this model comes from variations in atmospheric methane concentrations and Brazilian monsoon records which are in antiphase with boreal summer monsoon records (Ruddiman, 2006). In addition, Wang et al. (2010) conducted a study on stalagmite $\delta^{18}O$ ratios in two Chinese caves. These reflect precipitation during the Asian summer monsoon and are found to be concurrent with changes in the Greenland ice core $\delta^{18}O$ records which are paced by the precession.

In contrast to the Kutzbach et al. (1980) model, Clemens & Prell constructed a 350,000 year spanning record of the Indian summer monsoon. They based this record on five summer monsoon proxies from a number of Arabian Sea cores. The reconstructed summer monsoon record shows a lead of ~7,000 years to precession minima. Clemens and Prell (2003) infer from this that two processes exert an equal influence on the strength of the Indian summer monsoon: heating of the Asian Plateau which is at a maximum during periods when global ice volume is at a minimum and cross-equatorial latent heat transport from the Southern Indian Ocean which is at a maximum during precession maxima.

No decisive solution to this problem has been presented yet; Ruddiman (2006) suggested the summer monsoon strength index of Clemens & Prell (2003) was reflecting variables other than the strength of the Indian summer monsoon. In response, Clemens & Prell (2006) argued that Kutzbach's (1980) model did not incorporate land and ocean feedbacks and that comparing Indian monsoon records with the Chinese cave $\delta^{18}O$ record of Wang et al. (2010) was not a valid exercise since the boundary conditions of the two monsoon systems are probably different. Comprehensive reviews of the debate are given by Liu et al. (2009) and Wang et al. (2010).

Regardless of which hypothesis will in the end be the correct one, the phase relations of each of the two scenarios are very different from the lag Ziegler et al. (2010a) found between precession minima and productivity maxima. This indicates that maximal surface primary productivities in the Arabian Sea are primarily controlled by maximal strength of the AMOC rather than maximal Indian summer monsoon intensities.

4. Methods

4.1 Sampling

The PASOM 3 gravity core (fig. 3) was retrieved from a depth of 1172 mbss on the Murray Ridge (22°19.9 N, 63°36.0 E, fig. 1) during the PASOM cruise in January 2009. The six sections of the PASOM 3 core and the multi-core were opened using a rotating saw blade on a handheld Dremel device. After visually describing the core, half of each section was wrapped in plastic foil and stored at 4°C. The gravity core was then sampled at a resolution of 10 cm. The multicore was sampled at a resolution of 1 cm. After constructing an age model, a ~70 cm long section spanning 278-345 cm depth was sampled at cm resolution. All samples were weighed, dried at 40°C and water

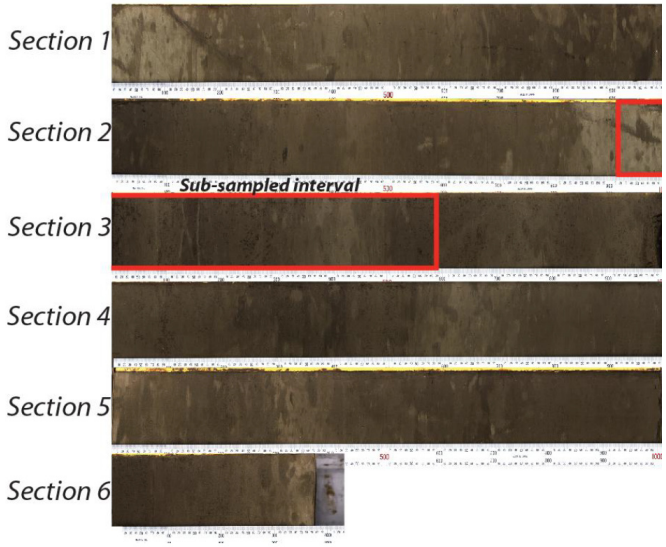

Figure 3; core PASOM 3. The length of the core is 537 cm and the sub-sampled interval is shown in sections 2 and 3. A lack of laminations indicates that the core is bioturbated throughout

content was estimated by weight loss on drying. At each depth interval, samples were taken for micropaleontology (min 5 cm^3), organic chemistry (min 10 cm^3) and inorganic chemistry (min 3 cm^3).

1.2 Micropaleontology
54 samples from the PASOM 3 gravity core, 68 samples from the high resolution section and 14 samples from the multicore were washed and sieved at fractions of 63 and 150 µm. After drying both fractions at temperatures of 40°C, the samples were weighed and split using the Otto microsplitter.

4.2.1 Stable oxygen and carbon isotope analysis
N. dutertrei is a planktonic foraminifer living at a depth of ~300 m (Shackleton et al., 1978; Reichart et al., 2002; Ishikawa et al., 2007). Approximately 30 hand-picked specimens of *N. dutertrei* at the 212-400 µm dry sieved fraction were processed for the stable isotope analysis. Only specimens which showed no sign of contamination or partial dissolution were selected. The dried specimens were weighed at a total of 300-1000 µg per sample. After weighing the specimens, stable oxygen and carbon isotope ratios were determined using a Fisons NA1500 NCS mass spectrometer. The standard used was the international standard IAEA-CO-1 (Stichler, 1995; Coplen et al., 2006). Whenever the size of the samples allowed, duplicate measurements were taken. The average difference of the seven duplicates was 0.1‰. Stable oxygen and carbon isotope ratios are reported in δ-notation relative to the international Pee Dee Belemnite standard (Emmerson & Hedges, 2008):

$$\delta^{18}O = \frac{^{18}O/^{16}O_{sample} - {}^{18}O/^{16}O_{standard}}{^{18}O/^{16}O_{sample}} \quad (1)$$

The $\delta^{18}O$ of *N. dutertrei* tests can be used to calculate sea surface temperatures during their growth period:

$$SST = 16.9 - 4.38*(\delta_c - \delta_w) + 0.10*(\delta_c - \delta_w)^2 \quad (2)$$

where δ_c is the $\delta^{18}O$ of foraminiferal calcite and δ_w is the $\delta^{18}O$ of the ambient sea water (Reichart et al., 2002, and references therein).

4.2.2 Deep-dwelling planktonic foraminiferal counts
Specimens of deep-dwelling planktonic foraminifers *Globorotalia crassaformis* and *Globorotalia truncatulinoide* in the >150 µm fraction were counted in all samples of the gravity core. Counts were normalized to the weight of the bulk sediment.

4.2.3 Pteropod counts
In the >150 µm fraction, pteropod fragments were counted for all samples of the gravity core. Counts were normalized to the bulk sediment weight.

4.2.4 Benthic foraminiferal record
Fifteen samples of the high-resolution interval were selected for benthic foraminiferal analysis. Samples which showed C_{org} maxima and minima were included in the analysis. For each sample, the >150 µm fraction was split to such an extent that approximately 300 specimens could be identified and picked. The program that was used for the statistical evaluation of the data was PAleontological STudies version 2.14 (PAST; Hammer, 2012). Diversity indices which were calculated were the Simpson Dominance ($D = \Sigma_i(n_i/n)^2$, where n is number of individuals of species i), Shannon H-diversity ($H = -\Sigma_i(n_i/n)*ln(n_i/n)$) and the equitability, which is defined as the Shannon diversity divided by the logarithm of the number of taxa (Hammer & Harper, 2006). A cluster analysis was carried out on the species which showed relative abundances of >2% in at least one sample and average abundances of >0.50% over the whole interval. Together, these species constitute 75-90% of the benthic assemblage. The paired group algorithm was used in combination with the Bray-Curtis similarity measure. On the selected species, a PCA was carried out. Following the method by Schmiedl et al. (2003), an oxygenation index has been constructed. This index is based on the normalized Shannon diversity and the relative abundances of marker species for oxygenation levels: Oxygenation = 0.5 * (H/(H+L)+Shannon diversity), with H = *O. umbonatus* + *P. bulloides* + *Hanzawaia spp.* + *C. ungerianus* + *P. murrhina* + miliolids and L = *Fursenkoina spp* + *C. oolina* + *R. semiinvoluta.*

4.3 Geochemistry
4.3.1 XRF analysis
Semi-quantitative element concentrations were obtained by X-Ray Fluorescence (XRF) core scanning. The archived half of core PASOM 3 was analyzed with the Avaatech XRF Core Scanner at

the Royal Netherlands Institution for Sea Research (NIOZ) following the procedure reported by Richter et al. (2007) and Tjallingii et al (2007). The core was covered with a 4 µm thin SPEXCerti Prep Ultralene foil and measurements were taken directly at the surface. The surface area of the measured section was 1x1 cm and measurements were taken at sampling times of 30 seconds and with voltages of 10, 30 and 50 kV with higher voltages being used for heavier elements. Elements measured were Al, Si, S, K, Ca, Ti, Mn, Fe, Zn, Br, Rb, Sr, Zr, Pb, Sn, I and Ba. Element counts were normalized in order to correct for differential porosity, water content and the concentrations of other elements affecting the whole dataset through the closed-sum effect (Tjalingii et al., 2008, and references therein). Usually, XRF records are normalized to Al (Shimmield & Mobray, 1991; Nagender et al., 1997; Reichart et al., 1997 & 2004; Wehausen & Brumsack, 2002; Wei et al., 2003; Langrock et al., 2004; Sun et al., 2008; Ziegler et al., 2010; Wang et al., 2010), but since Al is a very light element which cannot be accurately measured in wet cores using XRF (Ziegler et al., 2008), we avoided normalizations to Al. Instead, we performed a Principal Component Analysis on the XRF dataset and based on the loadings of the individual elements on the first axis, we selected the elements to which we would normalize the data, i.e. titanium and silicon were positioned on opposite ends of the axis, so we normalized the titanium to silicon concentrations.

4.3.2 Carbonate and organic carbon analysis

All samples of the high resolution interval were analyzed for carbonate and organic carbon contents. For each sample, a solution of ~10 ml 1M HCl was added to ~0.3 g of ground sediment. The samples were shaken for three hours and centrifuged at approximately 1600 rpm for six minutes; this procedure was repeated once with HCl and then twice more with demineralized water before weighing the residual sediment in order to calculate the carbonate loss. Organic carbon was measured using a CNS analyzer (Fisons NA 1500) and corrected for the loss of carbonate in the original samples.

4.3.3 Alkenone extraction

In order to estimate sea surface temperatures (SST) during the high resolution study window, the alkenone unsaturation ratio U^k_{37} was measured. Culture experiments have shown a correlation between this unsaturation ratio of the C_{37} alkenone and growth temperatures of the coccolithophoric species *Emiliani Huxleyi* which lives in the upper 25 m of the water column (Brassell et al., 1987; Prahl & Wakeham, 1987; Sikes et al., 1990; Villaneuva et al., 1997; Rostek et al., 1997; Sonzogni et al., 1997; Reichart et al., 2004; Conte et al., 2006). As this coccolithophore is a metropolitan species and the unsaturation index is not significantly affected by diagenesis (Sonzogni et al., 1997), the U^k_{37} index is a robust proxy to compare SST's worldwide and downcore.

The alkenone unsaturation ratio U^k_{37} was measured for every second sample from the high-resolution section. The resolution of the reconstructed SST's during the study window is ~250 years. Samples were oven dried, weighed and grounded. All lipids in the sediment were extracted using Accelerated Solvent Extraction (ASE). From each sample, between 1 and 6 mg of lipids were extracted using dichloromethane/methanol (DCM/MeOH; 9:1 v/v) on a Dionex 200 ASE extractor (Jansen et al., 2006). After drying under a constant flow of nitrogen the total lipid extract (TLE) was weighed and subsequently separated into three fractions: hydrocarbons, ketones and polarized hydrocarbons. This separation took place by elution through an alumina oxide (Al_2O_3) column with hexane/DCM (1:1 v/v), hexane/DCM (9:1 v/v) and hexane/MeOH (1:1 v/v). The three fractions were weighed again and from the keton fraction, the $C_{37:2}$ and $C_{37:3}$ chains were quantified using a Hewlett Packard 6890 Series Gas Chromatography (GC) system. An FID detector was used in combination with a 25 m long WCOT fused silica column with an inner diameter of 0.12 mm. Helium was used as carrier gas and for each sample, 1 µl of solvent was injected. The oven was programmed to start at 70ºC. After an initial rise of 20ºC/minute to 130ºC, the temperature rose further at 4ºC/minute to 320ºC, where it stayed for 20 more minutes. In addition to the keton samples, several samples of the polar and hydrocarbon fraction were processed as well, to validate complete separation of the fractions. The unsaturation index U^k_{37} is defined as follows:

$$U^k_{37} = \frac{(C_{37:2Me})}{(C_{37:2Me}) + (C_{37:3Me})}$$

From this unsaturation index, SST may be calculated using the following equation (Prahl & Wakeham, 1987; Müller et al., 1998; Reichart et al., 2002):

$$T = 29.412U^k_{37} - 1.147 \quad (3)$$

4.3.4 Sea Surface Salinity

By combining the SST and $\delta^{18}O$ data, sea surface salinity (SSS) can be calculated. Using the simple mathematical tool for solving quadratic functions ($X_{1,2} = (-b+/-\sqrt{(b^2-4ac)})/2a$) we can obtain the ($\delta^{18}O_c - \delta^{18}O_w$) in equation 2) by filling in the following equation:

$$(\delta^{18}O_c - \delta^{18}O_w) = \frac{(4.38 + \sqrt{(19.2 + 0.4*SST - 6.76)}}{(-2*SST + 33.8)}$$

Then, the SSS can be calculated using an empirical relationship between $\delta^{18}O_w$ and SSS in the Arabian Sea (Peeters, 2000; Reichart et al., 2004):

$$\delta^{18}O_w = -8.98 + 0.26 * SSS \quad (4)$$

5. Results

5.1 Low resolution study

5.1.1 Age model

Using the $\delta^{18}O$ records, the multi-core could not be tied to the piston core, so it is not possible to date the 28 centimeter of sediment which is contained within this interval. The age model for core PASOM 3 (fig. 4) is based on correlations with existing age models of deep-sea cores NIOP 463, 464 and MD04-2879 (Reichart et al., 1998; Ziegler, 2010a) which have been retrieved in the vicinity of the PASOM 3 core site. The existing age models of these cores are based on radioisotopically dated Globorotalia events (GEs), which are spikes of two deep-dwelling planktonic foraminifera (*G. crassaformis and G. truncatulinoides).* Occurrence of these taxa in the Arabian Sea is coeval with periods of major climatic cooling in the North Atlantic Ocean (Reichart et al., 1998; 2004; Schenau et al., 2002; Ivanova et al., 2003; Klöcker & Henrich, 2006; Ziegler et al., 2010). *G. truncatulinoides* and *G. crassaformis* reproduce at depths of 600 and 300 meters, respectively (Reichart et al., 1998; 2004). The overturning depth of the surface waters must thus be at least this large in order for standing stocks to occur. For the PASOM 3 age model (fig. 4), a number of different proxies were correlated to existing records of cores NIOP 463, 464 and MD04-2879. Ages for individual samples were calculated by linear interpolation between tie points. The average sedimentation rate is ~10 cm/kyr, with minima and maxima of 4 and 25 cm/kyr, respectively. These values agree very well with sedimentation rates found by Ziegler et al (2010) for core MD04-2879.

5.1.2 Micropaleontological proxies

A number of micropaleontological records were correlated to existing records from the Arabian Sea: the *N. dutertrei* $\delta^{18}O$ record, GEs and pteropod events (PEs) were used. In the $\delta^{18}O$ record (fig. 4), only the Last Glacial Maximum (LGM), Younger Dryas and IS 8 could be recognized. In the Arabian Sea, the $\delta^{18}O$ signal is affected by seasonality, upwelling and the winter monsoon, so it does not faithfully record high-frequency variations in the global climate and ice cover on the poles (Ziegler et al., 2010, and references therein). The overprint of the global climate can be recognized though, as the PASOM 3 $\delta^{18}O$ can very roughly be correlated to the precession curve (fig. 4). Pteropod fragments reflect the carbonate saturation state of the bottom waters via the Aragonite Compensation Depth (ACD; Reichart et al., 2004; Singh, 2007). In this way, they record periods when the OMZ was at a minimum. Four PEs can be recognized in the PASOM 3 record at ~64 ka, ~36 ka, ~22 ka and ~16 ka. Except for the peak at ~36 ka, these PEs largely coincide with the GE record. Reichart et al (1998) showed a 23-kyr cyclicity in the pteropod abundances of cores NIOP 464 and 463. This cyclicity is also present in the PASOM 3 core: pteropod events (PEs) and GEs are separated by roughly 23,000 years.

5.1.3 Geochemical proxies

In order to correlate records on a high resolution, a number of geochemical proxies obtained by XRF core scanning were used. These were sedimentary Sr/Ca, Ti/Si, K/Ti and Br records (fig. 9). Similar to the PE record, the Sr/Ca record is a proxy of the ACD and thus of the carbonate saturation state and oxygenation of the deep ocean (Reichart et al., 2004; Singh, 2007). The Ti/Si record reflects dust input into the Arabian Sea as titanium is more concentrated in the heavier mineral fraction (Shimmield & Mobray, 1991; Nagender et al., 1997; Reichart et al., 1997 & 2004; Wehausen & Brumsack, 2002; Wei et al., 2003; Langrock et al., 2004; Sun et al., 2008; Ziegler et al., 2010; Wang et al., 2010). Higher Ti/Si ratios thus indicate higher wind speeds and a more intense winter monsoon. The K/Ti record is a proxy for the intensity of the summer monsoon since potassium is leached from bedrock during chemical weathering and fixed in secondary minerals. Sediments are thus enriched in K during periods when the climate in the provenance region was wetter and in this way high K/Ti ratios reflect the precipitation and intensity of the summer monsoon (Wei et al., 2003). Bromine is a proxy for the organic matter content of the sediment (Ziegler et al., 2008) which, like the ACD, is influenced by paleoproductivity and past oxygenation of the deep ocean. Ziegler et al. (2008) found a close correlation between bromine and the organic carbon content of two deep-sea cores they studied. This relation is also reported by other authors (Reichart et al., 2004; Mayer et al., 2007). An empirical relation between the porosity and C_{org} exists: $C_{org} = e^{3.774*\ln(\text{porosity})-13.0122}$. The C_{org} and porosity data from the high resolution interval allowed us to test the equation on the PASOM 3 dataset. Calculated values for the C_{org} were too high; therefore the equation was adjusted: $C_{org} = e^{3.611*\ln(\text{porosity})-13.005}$. This resulted in a correlation coefficient of 0.36 between measured and modeled C_{org}. The new equation was applied to the porosities of the low resolution samples and the resulting C_{org} curve is shown in fig. 4. Minima at all Heinrich events are seen. Overall, the constructed C_{org} curve correlates very well with the normalized Br record.

5.2 High resolution study

5.2.1 Age model

The age model for the studied interval is based on a correlation of the PASOM 3 $\delta^{18}O$ and C_{org} records to the GISP 2 ice core $\delta^{18}O$ record (fig. 6). These profiles can be correlated in great detail: IS 8-12 and H4 are all present in the PASOM 3 $\delta^{18}O$ record and to some extent also in the C_{org} profile. This shows similar trends to the organic carbon records of the NIOP cores which are presented in Reichart et al. (1998). The difference in C_{org} is significantly smaller in core PASOM 3 though: whereas the stadial/interstadial C_{org} variation in core NIOP 455 is ~1.5% with a very large contrast of >4% at MIS 2.12, the variation in core PASOM 3 is on the order of 0.5% with a maximum of 1.5%. Stadial/

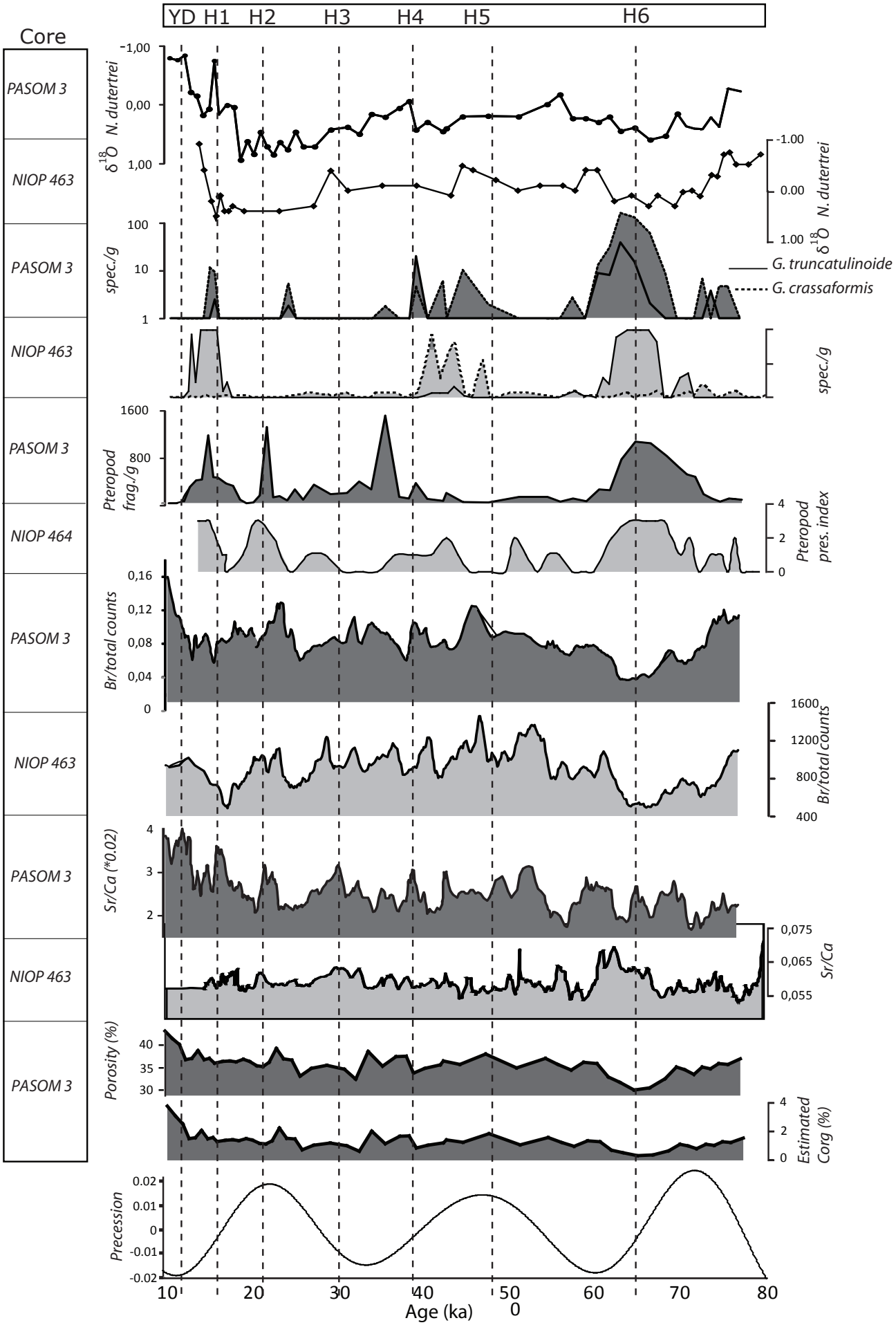
YD H1 H2 H3 H4 H5 H6
Core
PASOM 3
NIOP 463
PASOM 3
NIOP 463
PASOM 3
NIOP 464
PASOM 3
NIOP 463
PASOM 3
NIOP 463
PASOM 3
δ18O N. dutertrei
-1,00
0,00
1,00
-1.00
0.00
1.00
δ18O N. dutertrei
spec./g
100
10
1
G. truncatulinoide
G. crassaformis
spec./g
Pteropod frag./g
1600
800
Pteropod pres. index
4
2
0
Br/total counts
0,16
0,12
0,08
0,04
0
1600
1200
800
400
Br/total counts
Sr/Ca (*0.02)
4
3
2
0,075
0,065
0,055
Sr/Ca
Porosity (%)
40
35
30
Estimated Corg (%)
4
2
0
Precession
0.02
0.01
0
-0.01
-0.02
10
20
30
40
50
60
70
80
Age (ka)
0

Figure 4 (above); the age model for core PASOM 3. Different proxy records are correlated to reference cores NIOP 463, 464 and MD04-2804. Proxies used are N. dutertrei stable oxygen isotope ratios, Globorotalia truncatulinoide and Globorotalia crassaformis as well as pteropod fragment abundances and Br and Sr/Ca records. Also shown are the porosity and estimated C_{org} and the precession curve. Reference core data is from Ziegler et al. (2010)

interstadial shifts in $\delta^{18}O$ in the PASOM 3 core reach values of up to 0.8‰. Such shifts would suggest stadial/interstadial variations in SST of up to several degrees centigrade. Although no other Arabian Sea high-resolution records from this period are available, the magnitude of the variation in the $\delta^{18}O$ record seems to agree with lower resolution records such as NIOP 458, 463 and 464 (Den Dulk et al., 2000; Reichart et al., 2002).

5.2.2 Geochemical proxies

Surprisingly, the reconstructed SST profile (fig. 6) does not show the temperature variations of up to 3ºC which can be inferred from the $\delta^{18}O$ record. Interstadial reconstructed SSTs are ~25.5ºC and this figure drops to 24.5ºC during H4. This does not agree with Reichart et al (2002), who reconstructed SST in a similar fashion for core NIOP 458. They found interstadial values of ~24.5ºC which dropped to ~23ºC during H4. Before H4, temperatures were even lower, down to 22ºC at HE 5. Another study by Rostek et al. (1997) shows SSTs which are more similar to those found in this study. However, the core which these temperatures are based on is located near the outlet of the Red Sea, so it is questionable to what extent these records are supposed to be comparable. Also, differences in the age models may cause shifts in maxima and minima of the records. Another explanation for the high SSTs could be contamination during extraction or a badly calibrated gas chromatographer. Seven duplicate measurements have been taken and these show an average difference of 0.27ºC. This seems to indicate that the measurements by the gas chromatographer are relatively accurate. Also, the polar and hydrocarbon fractions which were processed in the GC show a proper separation of the three fractions.

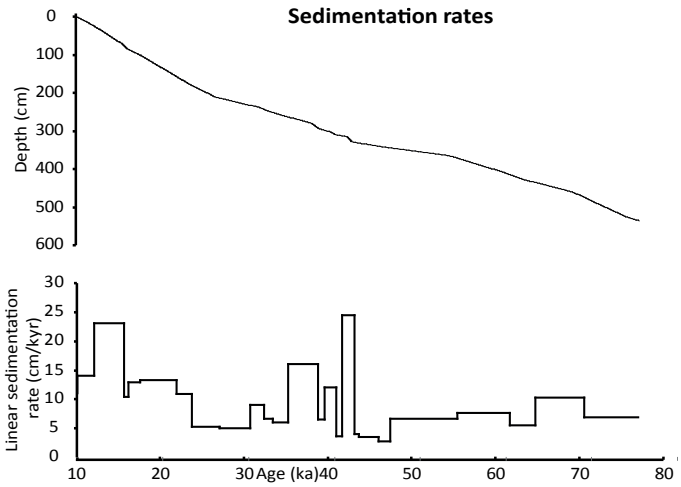

Figure 5; sedimentation rates of core PASOM 3

The reconstructed salinity curve for the study period is shown in figure 6. The salinity is very clearly anticorrelated with the C_{org} curve, with values of 37.2 PSU and 39.5 PSU during C_{org} maxima and minima, respectively. These values are slightly higher than salinities reported by Reichart et al. (2002). However, in this study, a stable oxygen isotope record of the benthic foraminifer *C. wuellerstorfi* instead of the planktonic foraminifer *N. dutertrei* was used. Differences may develop because the deep-sea salinity record mainly reflects changes in global ice volume while the surface record is also influenced by freshwater fluxes, evaporation and upwelling (Ziegler et al., 2010, and references therein). This introduces additional variability in salinity records which are based on $\delta^{18}O$ records of planktonic foraminifera. Additional geochemical proxies which are shown in figure 6 are the Sr/Ca, Ti/Si and K/Ti records. The Sr/Ca and K/Ti records show maxima and the Ti/Si record shows a minimum during H4.

5.2.3 Micropaleontology

5.2.3.1 Diversity, composition and cluster analyses

The benthic community during the studied interval shows distinct differences in composition. Respectively, maximum and minimum dominance and Shannon diversities are reached during MIS 2.12, 2.11 and 2.8. A pronounced maximum diversity and minimum dominance occurs during H4 (fig. 7). The cluster analysis yielded three groups (fig. 8). Group 1 contains *C. oolina, Fursenkoina spp., R. semiinvoluta* and *C. carinata*. This assemblage is similar to cluster 1 in Den Dulk et al. (2000), with the exception of *R. semiinvoluta*. Jorissen et al. (1995) studied two taxa from this assemblage (*Fursenkoina spp.* and *C. oolina)* in the Adriatic Sea where they burrow down towards additional sources of food on the oxic/anoxic boundary. When oxygen concentrations in the bottom water are being depleted, *C. oolina* and *Fursenkoina spp.* will probably migrate to shallower depths (Bernhard, 1992; Jorissen et al., 1995; Den Dulk et al., 1998; 2000; Schmiedl et al., 2003; Mazumder et al., 2003). Jannink et al (1998) reported that the intermediate infaunal species *R. semiinvoluta* requires a high food supply but does not tolerate anoxic bottom waters. They suggested that it may be a reliable marker species for the lower boundary of the OMZ. *C. carinata* is a shallow infaunal species which is often found in well oxygenated environments. A recent study by Duros et al. (2012) showed high abundances of *C. carinata* in the dead fauna below 1000 meters depth. However, it was never present in the live fauna. This species probably lives higher up on the slope and dead specimens may easily be transported along the slope to the deeper ocean because of their smooth, disc-like test. They

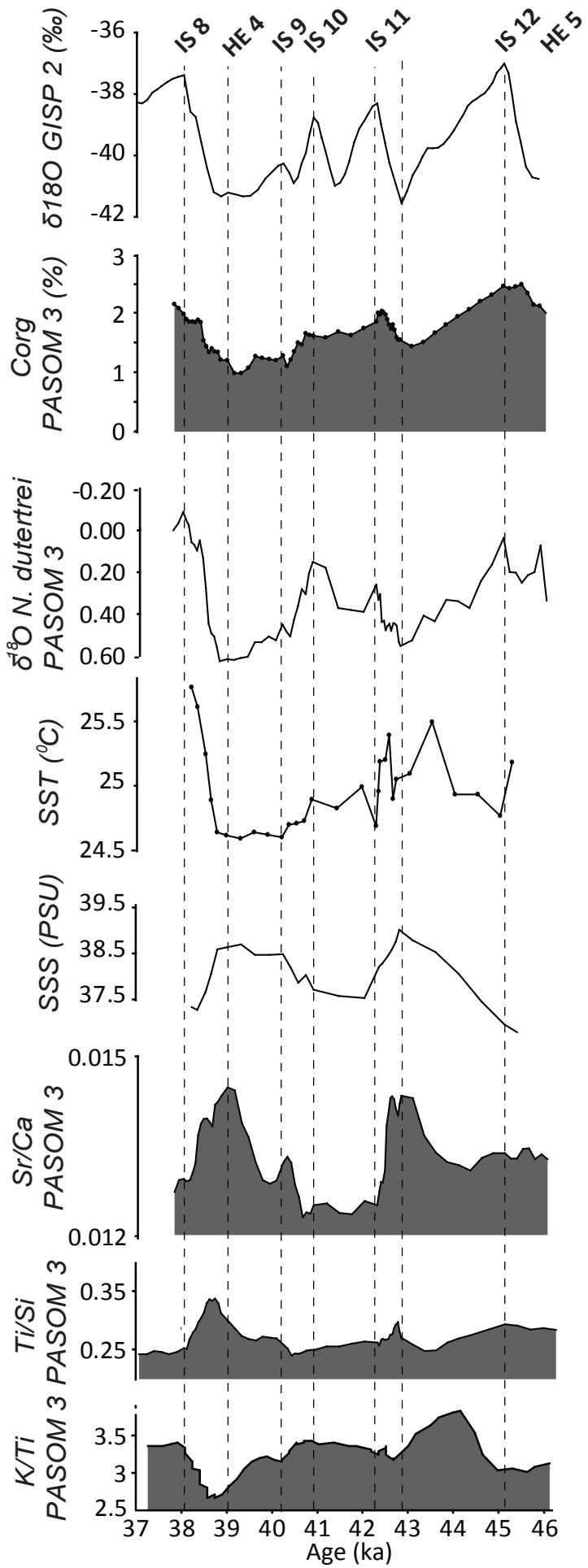

Figure 6; the high resolution age model for the sub-sampled interval in core PASOM 3. $\delta^{18}O$ and C_{org} records are correlated to the $\delta^{18}O$ record of ice core GISP 2. IS 8-12 and H4 can be recognized in the records. Also shown are the SST and SSS records and proxy records Sr/Ca (depth ACD), Ti/Si (winter monsoon strength) and K/Ti (precipitation summer monsoon)

may thus not accurately reflect the depositional environment.

The second cluster consists of *M. barleeanum, B. cf. dilatata and U. semiornata*. The latter two are shallow infaunal species which are numerically important species in the upper part of the Arabian Sea OMZ (Jannink et al., 1998; Den Dulk et al., 1998; Schumacher et al., 2007; Gooday et al., 2009). *M. barleeanum* is reported as having its preferred habitat below the lower boundary of the OMZ. It apparently has a large range in its average living depth and its position below the OMZ suggests it prefers altered organic matter (Jannink et al., 1998; Den Dulk et al., 2000).

All other species are contained within the third group. The majority of this group consists of species which live at intermediate depths in the sediment and are intolerant to oxygen depletion (Den Dulk et al., 1998; Hermelin & Shimmield, 1990). Examples are *C. ungerianus, C. subglobosa, G. inflata, O. umbonatus* and *Pullenia spp.* Another species in this assemblage is *U. peregrina.* This species is described by a number of authors as occurring just below the OMZ where oxygen concentrations are starting to rise (Hermelin & Shimmield, 1990; Jannink et al., 1998; Den Dulk et al., 1998; Schumacher et al., 2007).

Notable exceptions to the low-oxygen intolerant species in this assembly are *Globobulimina spp.* and *B. exilis.* The latter is described as a very productive species under conditions of low oxygen and high, pulse-like fluxes of labile organic matter (Jonkers, 1984; Jannink et al., 1998; Den Dulk et al., 1998; Jorissen et al., 2007). *Globobulimina spp.* lives deep in the sediment (>4cm) and feeds off slightly degraded organic matter near the oxic/anoxic boundary (Bernhard, 1991; Kitazato, 1994; Den Dulk et al., 1998; Mazumder et al., 2003; Jorissen et al., 2007). The whole list of microhabitats, ecological preferences and references of the benthic foraminifera is found in table 1.

5.2.3.2 Principal Component Analysis

The first two axis of the PCA explain 73% and 15% of the total variance; in table 2, the individual species scores are shown. Generally, the three assemblages recognized in the cluster analysis show very similar scores on the first two factors. Species which have high loadings on the first factor are *C. carinata, R. semiinvoluta, Fursenkoina spp., C. oolina* and *B. exilis.* Except for *C. oolina*, all these species belong to assemblage 1. Species

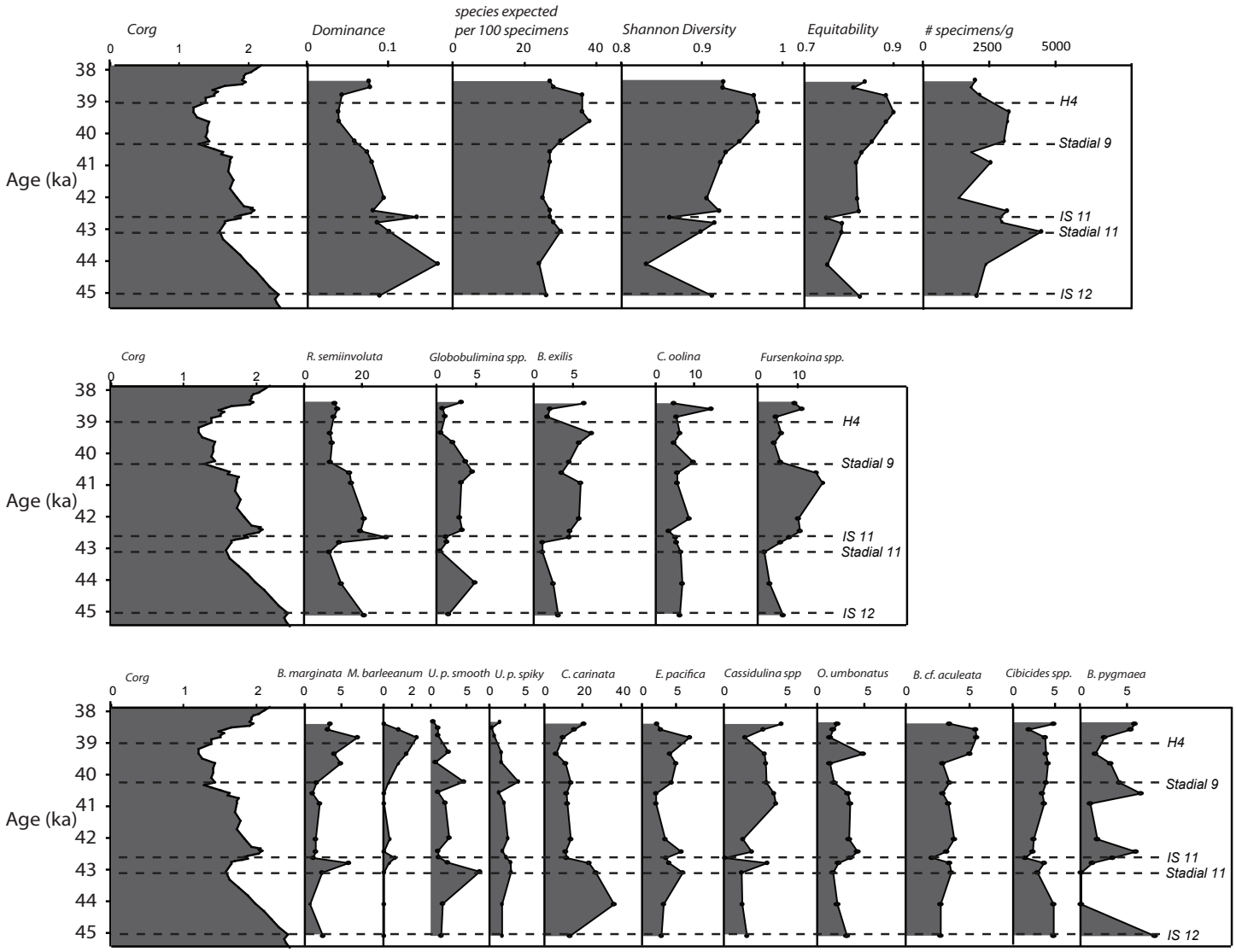

Figure 7; top) records of the C_{org}, dominance, rarefied diversity, Shannon diversity, equitability and the number of benthic foraminifers per gram of sediment. Middle) records of the C_{org} and relative abundances of deep infaunal benthic foraminifera which are adapted to low oxygen conditions. Bottom) records of the C_{org} and relative abundances of shallow infaunal benthic foraminifera which are intolerant to anoxic bottom waters

with high negative loadings on the first factor are *K. bradyi, S. bulloides, H. elegans, T. angulosa, Spiroplectammina sp., Lenticulina sp.* and miliolids. These species are intolerant to bottom water oxygen depletion and proliferate during periods of low C_{org} flux (Den Dulk et al., 1998; Von Rad et al., 1999). *H. elegans* and miliolid species are prone to dissolution during periods of high C_{org} flux because of their aragonite test (Den Dulk et al., 1998; Gooday et al., 2000; Jayaraju et al., 2010).

The highest scores on factor two are attained by *C. carinata, U. peregrina var. spiky, B. inflate, B. cf. aculeata* and *U. ungerianus.* All these species are epifaunal or shallow infaunal species which are not adapted to low bottom water oxygen contencentrations (Hermelin & Shimmield, 1991; Den Dulk et al., 1998; Jorissen et al., 1995; 2007). On the other end of the axis are *Fursenkoina spp., B. pygmaea, B. exilis, R. semiinvoluta, Globobulimina spp* and *B. alata.* All of these species occupy deep habitats in the sediment and most are tolerant to bottom water oxygen depletion (Kitazato, 1994; Den Dulk et al., 1998; Schumacher et al., 2007).

5.2.3.3 Interpreting the benthic clusters and PCA factors

Group 1 contains only a few taxa, which attain high abundances. The low diversity associated with this group is typical for benthic faunas living in oxygen-stressed environments (Hermelin & Shimmield, 1990; Den Dulk et al., 1998; Jannink et al., 1998). *C. carinata* is a species which is not expected to belong to this cluster as it is indicative of well oxygenated environments. However, due to its smooth, disc-like test it may not actually have lived at the core site but might have been transported from higher up the slope. When excluding *C. carinata* this cluster is thus indicative for the core of the OMZ (Bernhard, 1992; Jorissen

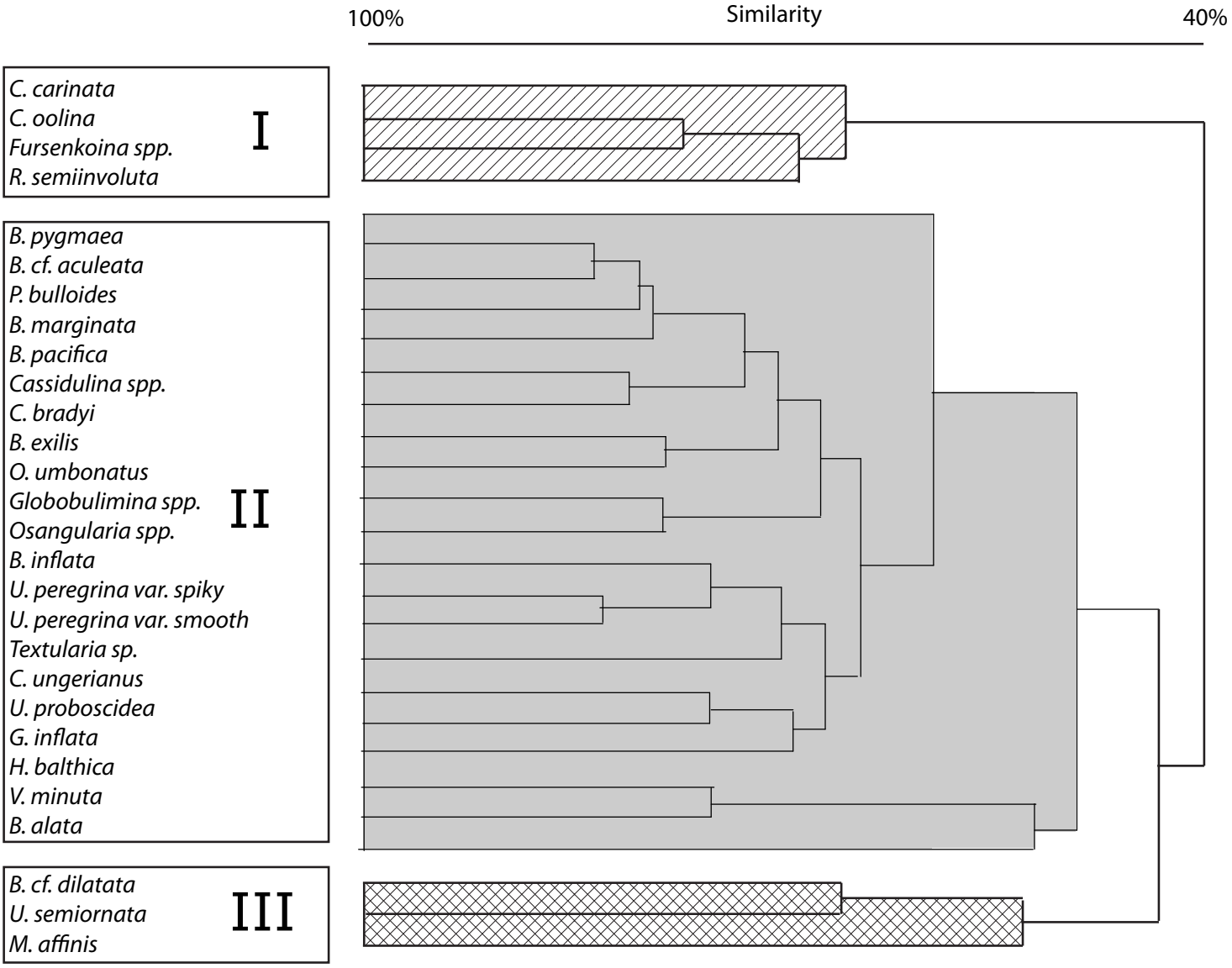

Figure 8; the benthic assemblages which were obtained with the cluster analysis. Assemblages are assigned Roman values I-III

et al., 1995; Den Dulk et al., 1998; 2000; Jannink et al., 1998; Schmiedl et al., 2003; Mazumder et al., 2003).
The shallow infaunal taxa in cluster 2 are tolerant to bottom water oxygen depletion (Jannink et al., 1998; Den Dulk et al., 1998; Schumacher et al., 2007; Gooday et al., 2009). Whereas the taxa from group 1 feed off organic matter which is preserved in the sediment, the taxa in this cluster profit directly from higher organic matter fluxes at the SWI. Especially during periods when bottom water ventilation decreases and species which are intolerant to low oxygen concentrations decline, these taxa will thrive. Probably, their reaction to an intensification of the OMZ is more immediate than the deep infaunal taxa in group 1.

Cluster 3 is a high diversity, low dominance assemblage. The species in this group are placed in three different faunas by Hermelin (1992), ranging from the lower part to just below the OMZ. The cluster found in this study is similar to cluster 1 in a study by Den Dulk et al. (1998) where they described it as a mixture between species indicative for moderately and well oxygenated bottom waters. In their study, *C. oolina* was also present in this group. This deep infaunal species is present near the oxic-anoxic front where it feeds off organic matter which is preserved in the sediment and would thus not fit in the assemblage. They argued that the presence of *C. oolina* in combination with these species is indicative of well oxygenated bottom waters with a deep oxic-anoxic boundary. In this study, *Globobulimina spp.* and *B. exilis,* instead of *C. oolina,* belong to this assemblage. It is here proposed that these taxa play a similar role *C. oolina* does in the study by Den Dulk et al. (1998). Cluster 3 is thus indicative of a well oxygenated, low C_{org} flux environment with oxygen penetration deep into the sediment.

PCA axes often represent one or more environmental parameters (Hammer & Harper, 2006). The high percentage of variance which is explained by the

Species	Microhabitat	Ecological preferences	Source
Fursenkoina spp	Deep	Hypoxic	1,2
C. oolina	Deep	Hypoxic	1,2
Globobulimina spp.	Deep	Hypoxic	1,6,7,8,16
B. exilis	Deep	Hypoxic	1,2,3,4,5,16
B. alata	Deep	Hypoxic	1,16
B. pygmaea	Deep	Hypoxic	1,12,16
B. cf. dilatata	Shallow	Hypoxic	1,2,10,11
U. semiornata	Shallow	Hypoxic	1,2,10,11
R. semiinvoluta	Intermediate-Deep	Oxic-Hypoxic	8,16
M. barleeanum	Shallow-Intermediate	Oxic-Hypoxic	1,2
B. marginata	Shallow-Deep	Oxic-Hypoxic	1,8,11
C. carinata	Shallow	Oxic	1,9
C. ungerianus	Shallow	Oxic	1,5,12,13
C. subglobosa	Intermediate	Oxic	1
G. inflata	Shallow	Oxic	1,5,17
O. umbonatus	Epifaunal-Shallow	Oxic	1,13,14,15,17
H. balthica	Shallow	Oxic	12,16,17
H. elegans	Shallow	Oxic	1,14,16
U. peregrina	Shallow	Oxic	1,2,6,8,10,12,13,16
C. bradyi	Shallow	Oxic	1,5,11
E. pacifica	Shallow	Oxic	1
K. bradyi	Shallow	Oxic	1,13
Miliolids	Shallow	Oxic	1,11,14,17
Pullenia spp.	Shallow	Oxic	1,5,13
S. bulloides	Shallow	Oxic	1,13
U. proboscidea	Shallow	Oxic	1

Table 1; Table showing the microhabitats and ecological preferences of the different benthic foraminifera. References: 1) Den Dulk et al. (2000); 2) Jannink et al. (1998); 3) Jonkers (1984); 4) Jorissen et al. (1995); 5) Jorissen et al. (2007); 6) Bernhard (1991); 7) Kitazato, (1994); 8) Mazumder et al. (2003); 9) Duros et al. (2012); 10) Schumacher et al. (2007); 11) Gooday et al. (2009); 12) Hermelin & Shimmield (1990); 13) Jorissen et al. (1998); 14) Jayaraju et al. (2010); 15) Rai et al. (2000); 16) Den Dulk et al. (1998); 17) Corliss & Chen (1988)

first PCA factor seems to indicate that this is the case in this study. Taxa from assemblage 1 and *B. exilis* which all thrive in anoxic environments have high loadings on this factor. The opposite end is occupied by species such as *H. elegans,* miliolids and *T. angulosa* which are intolerant to anoxia. This seems to indicate that the first PCA axis expresses an oxygenation gradient. Loadings of this axis compared with the C_{org} record support this (fig. 11): intervals with a high C_{org} correlate with high loadings of the first PCA factor. Since high C_{org} contents are coeval with periods when the Arabian Sea was more intense, the first PCA factor likely represents a gradient of bottom water oxygenation. It is important to note that this gradient is not only reflecting oxygenation, but probably also the flux of organic matter to the sediment and thus (export) productivity.

On opposite ends of the second PCA axis which explains a further 15% of the variance are deep and shallow infaunal taxa. This seems to indicate that it might be related to the microhabitat. Additionally, it may be that some of the ecological gradients which are reflected in the first factor have 'leaked' into this factor (Hammer & Harper, 2006). The highly negative loadings of *Fursenkoina spp., B. exilis* and *Globobulimina spp.* support this hypothesis, as they are species which thrive under dysoxic/anoxic conditions.

The cumulative relative abundances of the three clusters are shown in figure 11. From cluster 1, *C. carinata* was excluded because this species probably did not actually live at the core site but was transported from higher up the slope.

6. Discussion

6.1 Study limitations

In this section, the main liabilities of the used data are discussed. It is important to keep in mind that the geochemical proxies on which this climate

Table 2; loadings of all individual species on the first two PCA axes. Also shown are the average and maximum abundances of the species

Species	PCA 1	PCA 2	Average	Max
C. carinata	53.39	22.83	15.58	36.49
R. semiinvoluta	41.61	-23.97	12.48	32.31
F. bradyi	18.86	-9.61	7.60	16.15
C. oolina	14.05	1.91	6.41	14.43
B. exilis	4.66	-3.42	4.08	7.60
E. pacifica	3.73	1.49	3.84	6.93
B. pygmaea	2.81	-4.60	3.45	8.16
B. cf. aculeata	0.41	1.25	3.01	5.94
O. umbonatus	0.21	-2.53	2.68	4.80
B. marginata	-0.46	2.04	2.87	7.26
Cassidulin. spp.	-0.80	0.79	2.59	4.56
Globobulimina. spp.	-0.85	0.02	2.26	4.91
P. bulloides	-1.35	0.19	2.52	5.61
B. inflata	-1.92	2.65	2.30	5.34
U. peregrina var. spiky	-2.31	3.00	2.04	6.98
C. ungerianus	-2.42	1.46	1.84	4.96
U. peregrina var. smootl	-2.44	0.56	1.95	4.01
Osangularia sp.	-2.78	-0.17	1.83	4.68
U. proboscidea	-3.98	1.34	1.56	2.81
C. bradyi	-4.06	0.41	1.76	3.51
Textularia. sp	-4.35	1.97	1.45	4.67
G. inflata	-5.26	0.98	1.39	3.16
B. cf. dilatata	-6.24	-0.01	0.91	3.85
B. alata	-6.46	-1.75	0.88	2.41
H. balthica	-6.93	0.13	0.72	2.06
V. minuta	-7.01	0.07	0.69	2.06
U. semiornata	-7.33	-0.43	0.69	2.15
M. barleeanum	-8.38	-0.09	0.51	2.31
Miliolids spp.	-8.51	0.39	0.35	1.65
Lenticulina sp.	-8.93	0.06	0.33	2.00
Spiroplectammina sp.	-9.16	0.31	0.25	2.31
T. angulosa	-9.37	0.40	0.11	1.00
H. elegans	-9.38	0.18	0.19	1.32
S. bulloides	-9.45	0.58	0.09	1.33
K. bradyi	-9.58	-0.09	0.06	0.34

reconstruction is mainly based are semiquantitative records. They have not been obtained analytically and it is not possible to convert the data to absolute concentrations. Data obtained with XRF core scanners are subject to a number of problems. One of these is the closed-sum effect. The sum of the concentrations of all measured elements equals unity (Richter, 2006; Weltje & Tjallingii, 2008). Therefore, if one element becomes less abundant, abundances of all other elements are proportionally increased. Correcting for this problem can be done by normalizing element counts to either the total counts in a particular XRF scanning run or to other elements.

Another problem in XRF data acquisition is the effect of water content on mainly the lighter elements (Al and Si, Weltje & Tjallingii, 2008). An illustration of this is a study by Ziegler et al. (2010). They correlated analytically obtained aluminum concentrations with the Al profile obtained with an Avaatech XRF core scanner. The correlation coefficient they found was only 0.38, indicating a very high noise/signal ratio.

A third problem in XRF data acquisition may arise when analyzing wet cores. When measuring cores, a thin water film may develop underneath the thin foil with which the core halves are covered (Tjallingii, 2007; Weltjes & Tjallingii, 2008; Hennekam & de Lange, 2012). Hennekam & de

Figure 9 (below); Downcore records of several geochemical proxies obtained with an XRF core scanner: K/Ti (precipitation summer monsoon), Ti/Si (intensity winter monsoon), Sr/Ca (depth ACD) and Br (organic carbon). Also shown is the Al record.

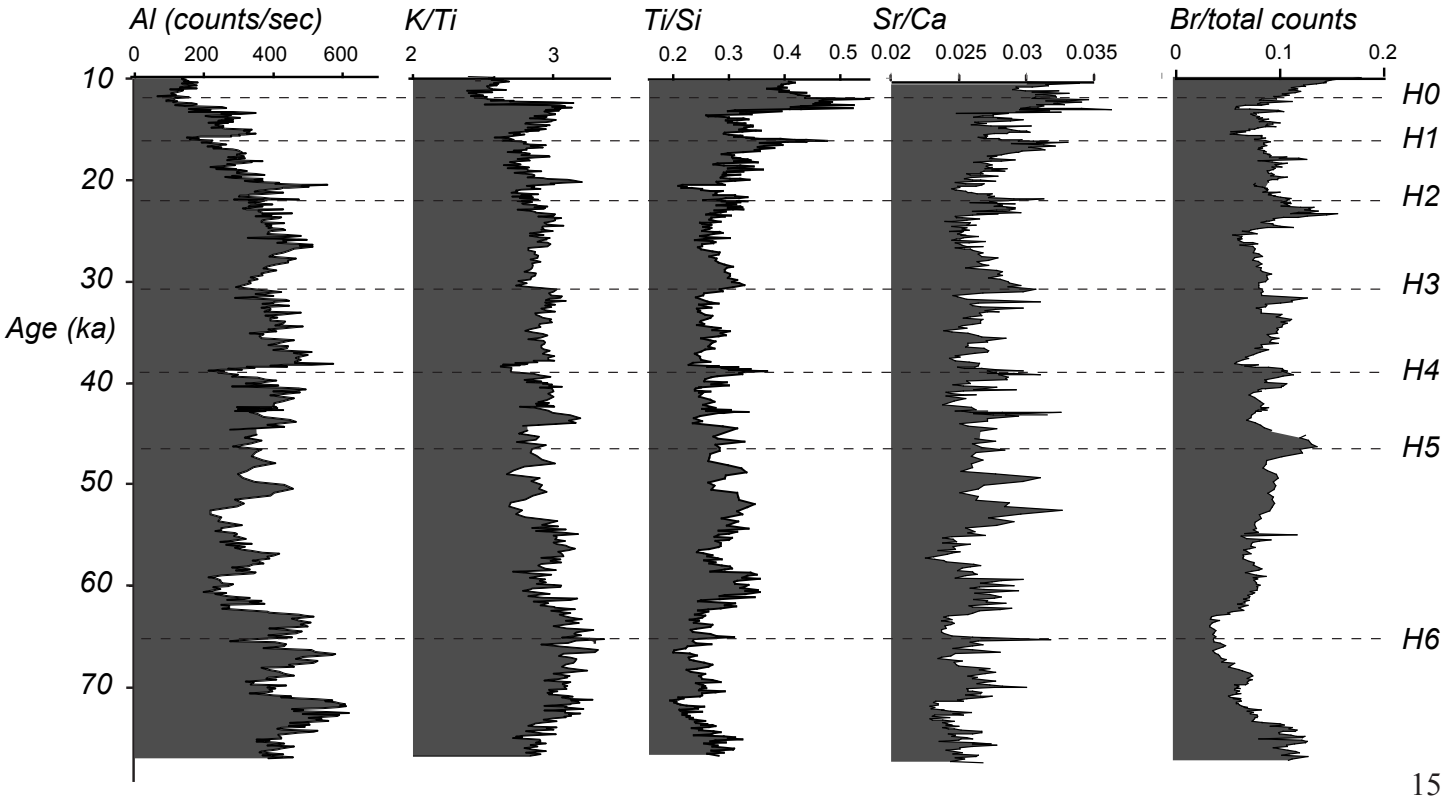

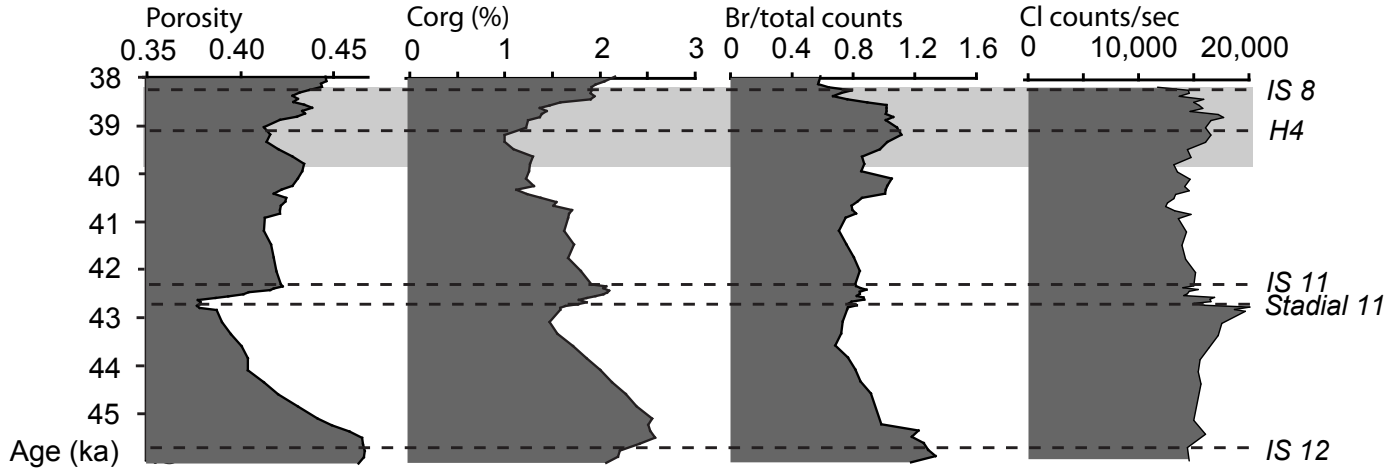

Figure 10; Downcore profiles of porosity, C_{org}, Br and Cl. The former three records are correlatable throughout the section except during H4, shown as a grey band

Lange (2012) showed that Br, Cl and S show very similar downcore profiles. All three elements are predominantly present in pore waters, so variations in these elements were largely attributed to variations in the water film thickness. This introduced variability may thus lead to deviations in paleoenvironmental reconstructions (Hennekam & de Lange). An example of this may be seen in figure . During H4, the organic carbon profile shows a broad minimum while a peak in Br is observed. This is contrary to expectations since Ziegler et al. (2008) showed a near-perfect correlation between these two records. However, the Cl profile which is also shown in figure 10 shows a peak during H4. This suggests that the mismatch between the Br and C_{org} records at this interval is caused by an anomalously thick water film. In figure 12, the C_{org} and Br profiles of five Murray Ridge cores taken at increasing depths are shown. Small discrepancies between the C_{org} and Br records in these cores probably arise from variations in the thickness of the water films.

6.2 OMZ variability during the last glacial

From the different biological and geochemical proxies, a reconstruction of the regional climate during the last glacial can be made. The high spatial resolution of the XRF data results in a temporal resolution of ~150 years. The resolution of the pteropod and Globorotalia abundances and *N. dutertrei* $\delta^{18}O$ record is much lower (~1000 years). The coldest stadials were H1, H4 and H6 since overturning depth in the Arabian Sea was only during these periods sufficiently large to support standing stocks of *Globorotalia spp.* In addition, the ACD was the deepest during these periods, as shown by high pteropod abundances in the sediment. During stadials, the geochemical proxies show a weakening and strengthening of the summer and winter monsoon, respectively. Lower K/Ti values indicate a decrease in clay content derived from chemically weathered bedrock (Wei et al., 2003). This indicates a drier and colder continental climate. Peaks in the Ti/Si record show an increase in wind speeds over the Arabian Sea related to an intensification of the winter monsoon (Reichart et al., 1997).

It is possible though, that a Heinrich event was missed due to the relatively low resolution of the *Globorotalia* and pteropod records. Roche et al. (2004) used a climate model to calculate that the duration of H4 was 250 +/- 150 years. Sedimentation rates at the core site during H4 were ~8 cm/kyr so an event which took 400 years would result in a ~3 cm thick layer. With a sampling resolution of 10 cm, such an event could easily be missed, even when accounting for a 'smoothing out effect' of the GE by bioturbation. However, the GEs at H1 and H6 agree with the GE record Reichart et al. (2002) presented, so all GEs have probably been captured in the samples of the low resolution interval.

6.3 Orbital control on OMZ variability

GEs and PEs occur during periods when the Arabian Sea OMZ is at it least intense. In figure 4, four GEs and PEs can be recognized: at ~64 ka, ~39 ka, ~22 ka and ~16 ka. The ~23,000 year intervals between these events (except for the one at ~22 ka) indicate that periods of minimum OMZ intensity are paced by the precession. A cross-correlation to the precession curve (figure 4) reveals a consistent ~7,000 year lag of these OMZ minima to precession maxima. This corresponds with the lag Ziegler et al. (2010) found in cores MD04-2879 and NIOP 463. The similar lag which has been found for minimum intensities of the AMOC during the Late Pleistocene indicates that variability in the Arabian Sea OMZ is mainly controlled by changes in the AMOC.

The bromine and estimated C_{org} records of core PASOM 3 (fig. 4) show distinct minima during H1, H4 and especially H6. This antiphase with the GE and PE records is also noted by Ziegler et al. (2010). In addition, Reichart et al (1998) reported a ~6,000 year time lag between precession and organic carbon maxima in a number of Arabian Sea cores. It thus seems that maxima in AMOC intensity lead to maximal productivities and OMZ intensities in the Arabian Sea. Apparently, the

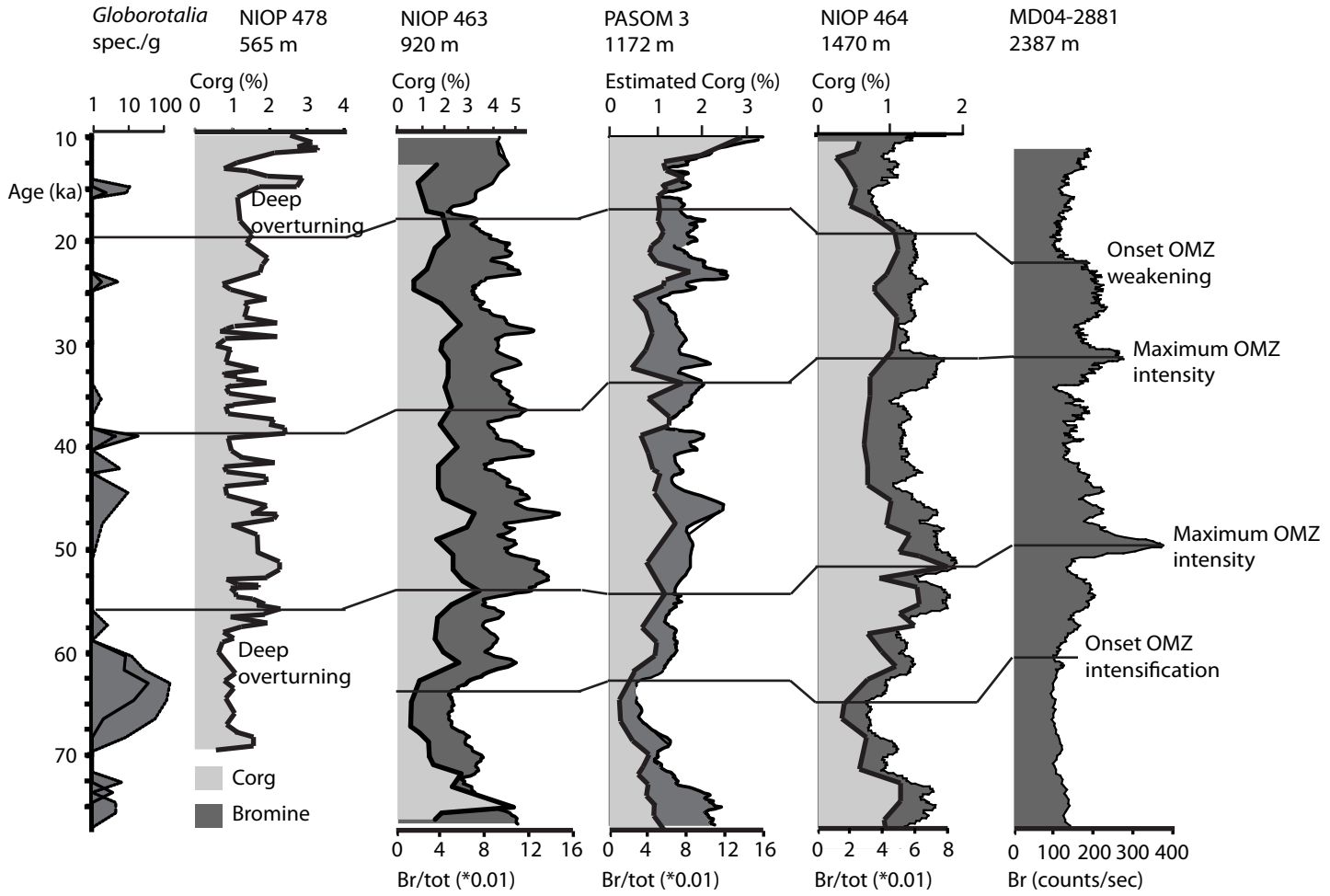

Figure 11; Br and Corg records of five Murray Ridge cores, ranging from 565 to 2387 m depth. The records can be correlated in great detail; a number of peaks and troughs is correlated. These correlations show the expanding OMZ over the course of several thousands of years. Also shown is the PASOM 3 Globorotalia record; GEs can coincide with minima in the shallowest site, reflecting deep overturning during these periods. Data is from den Dulk et al. (1998), Reichart et al. (2004) and Ziegler et al. (2010)

total nutrient budget in the Arabian Sea is more important in controlling productivity and deep water oxygenation than the rate at which these nutrients are overturned.

Alternatively, the Indian summer monsoon may have played a large role in determining maximum surface productivities in the Arabian Sea. Reichart et al. (1998) discussed that the 6,000 year lag they found between precession minima and productivity maxima might be related to maximum annual productivities. In this way, maximum productivities would not be controlled by maximal summer monsoon intensities, but by the length of the summer monsoon and upwelling season. Thus, maximal late (September), rather than early (June) summer insolation would result in maximal surface productivities. An insolation maximum at September 21st corresponds to a ~5,700 year lag between a precession minimum and maximal length of the productivity season. However, the average lag of ~7,000 years which has been found in the PASOM 3 record seems to indicate that although the length of the upwelling season may have played a role in the annual productivities in the Arabian Sea, changes in the AMOC probably were the overriding control on productivities during the last glacial.

6.4 Spatial and temporal variability in the Arabian Sea OMZ

Since the late 90's, a lot of deep-sea records have become available from the Arabian Sea (Reichart et al., 1997, 1998, 2002, 2004; Den Dulk et al., 1998; 2000; Ziegler et al., 2008, 2010a, 2010b). This large database allows us to constrain spatial and temporal variations in the Arabian Sea OMZ by comparing the different records. In figure 12, five of the Murray Ridge records are shown: cores NIOP 478 and 463, PASOM 3, NIOP 464 and MD04-2881, retrieved at depth of 565, 920, 1172, 1470 and 2387 m respectively (Den Dulk et al., 2000; Reichart et al., 2004; Ziegler et al., 2010b). The C_{org} and bromine profiles of these cores are shown and several maxima and minima have been correlated throughout the records. A number of observations can be made by comparing the different profiles: during H6, a broad C_{org} and Br minimum can be seen in all the records. The minimum is followed by a stepwise rise in C_{org} content to a peak, reflecting the expansion of the OMZ over the core sites (Reichart et al., 1998; Van der Weijden et al.,

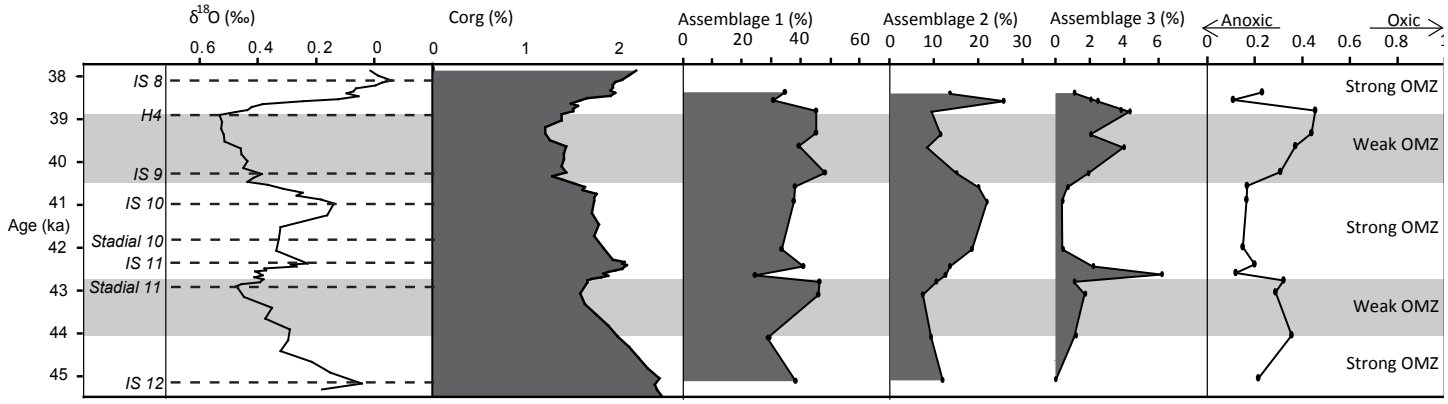

Figure 12; The $\delta^{18}O$, C_{org} and loadings of the first PCA factor are shown. Also shown are relative abundances of the three benthic assemblages which were obtained with the cluster analysis and the oxygenation index which is related to the Shannon diversity and abundances of several marker species (after Schmiedl et al., 2003). Two periods when the OMZ was substantially weakened are recognized.

1999). This intensification is seen to occur later in the bottom waters overlying the deeper sites: whereas organic carbon contents start to increase at the NIOP 463 site (920 m) at ~64 ka, they do not rise at the deepest site (MD04-2881, 2387 m) until ~60 ka. From this, we may interpret that it took the OMZ approximately 4,000 years to expand to maximal depths after H6. A similar observation is made at H4, where the lag of the deepest cores is even larger.

Remarkably, organic carbon contents in the shallowest site (NIOP 478, 565 m) start to increase very late during the period surrounding H6. This probably reflects a continuous burn-down of organic matter which is related to deep convectional overturning. This is clearly seen when comparing the NIOP 478 C_{org} and PASOM 3 *Globorotalia* records (fig. 12). At every GE in the PASOM 3 record, there is a sharp minimum in the NIOP 478 C_{org} profile. Another notable feature in the records is the transition to the Last Glacial Maximum (LGM) at ~20 ka. The deepest site drops to low Br values already at ~22 ka, while at shallower sites this drop occurs several thousands of years later. This probably reflects the shrinking of the OMZ during the LGM which becomes visible first in the deepest record.

Another observation can be made by comparing the PASOM 3 core with the two cores lying directly above and below it (NIOP 463 and 464). Whereas the NIOP 463 records show sharp maxima and minima, the Br and C_{org} profiles are much smoother in core NIOP 464. The PASOM 3 record seems to be a transition between these two, reflecting the closer proximity of the PASOM 3 core site to the core of the OMZ. Since no benthic foraminiferal data is available from the low resolution study, it is not possible to say whether the lower boundary of the OMZ dropped below the core site at 1172 m.

6.5 High resolution interval: environmental reconstruction

In general, it seems that bottom waters at the core site during the studied period were never truly anoxic. Throughout the period, the oxyphilic assemblage continues to make up a significant portion of the total benthic assemblage with total relative abundances never dropping below 30% (fig. 11). *C. ungerianus* is a marker species of well oxygenated bottom waters which Jannink et al. (1998) report as being intolerant to oxygen concentrations below 2.1 ml/l. Since this species is present in every analyzed sample (fig. 7) and the boundary of the OMZ consists of waters containing oxygen concentrations of 0.5 ml/l, we may conclude that during the high resolution period, the lower boundary of the OMZ was located above the core site.

Furthermore, when comparing the *N. dutertrei* $\delta^{18}O$ and C_{org} records with the benthic assemblage data, it can be observed that the benthic fauna was highly sensitive to changes in oceanic conditions in the overlying water column. The composition of the benthic assemblage changes with very little or no lag to these changes. The organic carbon content seems to be related to the intensity of the OMZ. Organic carbon burial efficiency is known to be positively influenced by higher sedimentation rates (Van der Weijden et al., 2006). However, higher sedimentation rates occur in periods with low sedimentary C_{org} contents, so this cannot satisfactorily explain the variation in C_{org}. Enhanced inputs of terrestrial organic matter are also very unlikely at the core site (Reichart et al., 1998). The C_{org} record must thus be related to the OMZ intensity.

During the studied period, there were two intervals during which the OMZ was minimally developed. These intervals occur before and during stadial 11 and H4. Both intervals show high Sr/Ca peaks, indicating an increased ACD and a well oxygenated deep ocean. This is supported by minima in the C_{org} record and a high diversity, low dominance benthic fauna, in which oxyphilic taxa from cluster

1 dominate. H4 is a more severe stadial, which is indicated by lower C_{org} and SSTs, a higher SSS and maximal and minimal values in the Ti/Si and K/Ti records, respectively. The winter monsoon was thus intensified while enhanced chemical weathering and less runoff indicate that precipitation of the summer monsoon was minimal. However, when using the geochemical data in the interval surrounding H4, care must be taken as probably the water film underneath the foil was anomalously thick during the XRF measurements, resulting in incorrect concentrations of especially the lighter elements (Tjallingii et al., 2008; Hennekam & de Lange, 2012).

The composition of the benthic assemblage is roughly similar in both cold periods: cluster 1 dominates the benthic fauna with relative abundances of ~40%. Smaller contributions are made by clusters 2 and 3 (~10% and ~4%, respectively). Species which indicate well oxygenated bottom waters are more abundant during H4, resulting in a higher oxygenation index (fig. 11). All deep infaunal species (*R. semiinvoluta, Globobulimina spp., C. oolina, Fursenkoina spp.* and *B. pygmaea)* show minimal abundances in the cold periods, reflecting the higher oxygen concentrations in the bottom waters and the subsequent reduced sedimentary C_{org} at the depths where these taxa were living (Jorissen et al., 1995; Jannink et al., 1998).

Interestingly, *B. exilis* shows a maximum during H4. Since the ecological preferences of *B. exilis* are the same as the other deep infaunal species, the *B. exilis* record is expected to be similar to these records (Jonkers, 1984; Jannink et al., 1998; Den Dulk et al., 1998; Jorissen et al., 2007). This species is known to be able to reproduce very quickly (Jannink et al., 1998). Therefore, under optimal circumstances, its relative abundance in the assemblage may be very high. Therefore, it may be that changes in *B. exilis* abundance have to be on the order of tens of percentages to be significant. In the study period, it never reaches relative abundances higher than 6%, so maybe the peak during H4 is just a slight deviation of the relatively low background values. When normalizing the *B. exilis* to the sediment weight, the H4 peak becomes much lower as well; the peak in the relative abundance may thus also be an artifact related to this.

The interstadial periods surrounding the well oxygenated intervals show low Sr/Ca and high C_{org} values, indicating that the deep ocean was badly ventilated. The benthic fauna shows high dominances while diversities are lower during these periods. Cluster 2 shows large peaks during IS 10/11 and 8 while the cumulative abundance of cluster 1 shows slight decreases. The oxygenation index shows a large decrease during these periods. In the individual abundance records (fig. 7), a spike in the *B. marginata, M. barleeanum* and *B. pygmaea* records is seen at the same time as organic carbon contents start to rise. These opportunistic species probably represent the transition to low-oxygen conditions when the OMZ was expanding (Jannink et al., 1998; Jorissen et al., 1998; Mazumder et al., 2003). During C_{org} maxima at IS11 and 8 when the OMZ had expanded to a maximum, these taxa decline to background values.

6.6 Processes controlling OMZ variability during the high resolution interval

Using the SST, SSS and $\delta^{18}O$ data, we can attempt to reconstruct the processes which led to the shrinking of the OMZ during stadial 11 and H4. Surface water salinities increase during the cold stadials by ~2.5 PSU (fig. 6). Together with the decrease in K/Ti values, this reflects reduced runoff due to a weakened summer monsoon and/or increased evaporation at the surface (Schulte et al., 1999; Reichart et al., 2002). During H4 and stadial 11, reconstructed SSTs drop by only 1°C. From the $\delta^{18}O$ curve, a cooling of ~3°C can be calculated. However, the reconstructed SST reflects temperatures at the <25 m depth range while the $\delta^{18}O$ curve reflects much deeper changes at ~300 m. The difference could be explained by a difference in growth season (Poulton et al., 2010).

During stadial 11 and H4, the cooling of the surface waters in combination with the increased salinities caused the picnocline to deepen, thereby increasing convectional overturning of the surface waters. In this way, the top of the OMZ was eroded. It is unlikely that the overturning depth reached to the lower boundary of the OMZ (Schulte et al., 1999) so probably, other factors contributed to the shrinking of the OMZ during stadial 11 and H4. A weakening of the AMOC during these periods reduced the advection of deep, nutrient rich waters, decreasing surface and export productivities (Ziegler et al., 2010a). The reduced summer monsoon (fig. 6) probably further decreased annual surface productivities. At the same time, oxygen concentrations in the Indian Central Water increased (Schmittner et al., 2007). All these factors combined to substantially weaken the OMZ. During the warm interstadials, an increase in deep water nutrient advection, enhanced productivities due to the intensified summer monsoon, stratification of the surface waters and a depletion of oxygen in the Indian Central Waters combined to restore the OMZ intensity. However, as the benthic data indicates, the base of the OMZ never dropped below the core site at 1172 m during the studied period.

7. Conclusion

The Arabian Sea OMZ exhibits strong variations over the core site during the last 75,000 years. In the proxy records, Heinrich events can be recognized as increases in the surface water overturning depth and in the ACD, reduced sedimentary organic carbon contents, weakened summer monsoons and intensified winter monsoons. The three periods where OMZ intensity is at a minimum show a 7,000 year lag with maximum precession. This

indicates that the Arabian Sea OMZ variability is predominantly controlled by changes in the Atlantic Meridional Overturning Circulation. Comparing the PASOM 3 C_{org} and bromine records with similar records from stations NIOP 463 and 464 at 920 and 1470 m depth, respectively, shows the proximity of the PASOM 3 site to the lower boundary of the OMZ. Unfortunately, it is not possible to say whether the lower boundary dropped below the core site at 1172 m during the last glacial because we have not analyzed the benthic foraminiferal assemblage in the low resolution study.

In the high resolution interval, millennial-scale OMZ variability which can be correlated to the global climate signal in the GISP 2 ice core is observed. Bottom waters over the cores site were well oxygenated during two periods: during stadial 11 (~44-42.8 ka) and around H4 (~40.5-39 ka). These periods are characterized by a high diversity, low dominance benthic faunal assemblage. Abundances of deep infaunal taxa which are feeding off degraded organic matter on the oxic/anoxic boundary decreased while shallow infaunal species which are intolerant to anoxic bottom waters became more abundant. Results show that the lower boundary of the OMZ never dropped below the core site during the studied period. Sea surface salinities and temperature changes during H4 are probably not sufficient to have caused vertical mixing to the base of the OMZ. In addition to an increase in convectional overturning depth, reduced productivity and advection of oxygen-rich Indian Central Water related to the weakening of the AMOC are induced to explain the weakening of the OMZ during H4.

8. Acknowledgements

First of all, I'd like to express my thanks to Dr. Karoliina Koho, who was always there to help me with both the practical and theoretical work during this thesis. I'd also like to thank Dr. Gert-Jan Reichart for giving me the opportunity to work on such an ambitious project. I'm also very thankful to Dominika Kasjaniuk, Dr. Klaas Nierop, Dr. Martin Ziegler, Dr. Lennart de Nooijer, Arnold van Dijk and Dr. Tom Jilbert for providing data, assisting me with the labwork and discussing the subsequent results.

9. References

Almogi-labin, A., Schmiedl, G., Hemleben, C., Siman-tov, R., & Segl, M. (2000). The in ¯ uence of the NE winter monsoon on productivity changes in the Gulf of Aden , NW Arabian Sea , during the last 530 ka as recorded by foraminifera. *Marine Micropaleontology*, *40*.

Altabet, M. a, Higginson, M. J., & Murray, D. W. (2002). The effect of millennial-scale changes in Arabian Sea denitrification on atmospheric CO2. *Nature*, *415*(6868), 159-62.

Altabet, M.A., Francos, R., Murray, D.W., Prell, W. L. (1995). Climate-related variations in denitrification in the Arabian Sea from sediment 15N/14N ratios.pdf. *Letters to Nature*, *373*(February), 1995.

Barker, T. (2007). *Climate Change 2007: An Assessment of the Intergovernmental Panel on Climate Change* (pp. 12-17).

Bernhard, J. M. (1992). Benthic foraminiferal distribution and biomass related to pore-water oxygen content: central California continental slope and rise. *Deep Sea Research Part A. Oceanographic Research Papers*, *39*(3-4), 585-605.

Böning, P., & Bard, E. (2009). Millennial/centennial-scale thermocline ventilation changes in the Indian Ocean as reflected by aragonite preservation and geochemical variations in Arabian Sea sediments. *Geochimica et Cosmochimica Acta*, *73*(22), 6771-6788.

Brand, T. D., & Griffiths, C. (2009). Seasonality in the hydrography and biogeochemistry across the Pakistan margin of the NE Arabian Sea. *Deep Sea Research Part II: Topical Studies in Oceanography*, *56*(6-7), 283-295. Elsevier.

Brassell, S.C., Eglinton, G., Marlowe, I. T., Pflaumann, U., & Sarnthein, M. (1986). Molecular stratigraphy: a new tool for climatic assessment. *Nature*.

Bulow, S. E., Rich, J. J., Naik, H. S., Pratihary, A. K., & Ward, B. B. (2010). Denitrification exceeds anammox as a nitrogen loss pathway in the Arabian Sea oxygen minimum zone. *Deep Sea Research Part I: Oceanographic Research Papers*, *57*(3), 384-393. Elsevier.

Böning, P., & Bard, E. (2009). Millennial/centennial-scale thermocline ventilation changes in the Indian Ocean as reflected by aragonite preservation and geochemical variations in Arabian Sea sediments. *Geochimica et Cosmochimica Acta*, *73*(22), 6771-6788.

Clemens, S. C., & Prell, W. L. (2003). A 350,000 year summer-monsoon multi-proxy stack from the Owen Ridge, Northern Arabian Sea. *Marine Geology*, *201*(1-3), 35-51.

Clemens, S. C., & Prell, W. L. (2007). The timing of orbital-scale Indian monsoon changes. *Quaternary Science Reviews*, *26*(3-4), 275-278.

Conte, M. H., Sicre, M.-A., Rühlemann, C., Weber, J. C., Schulte, S., Schulz-Bull, D., & Blanz, T. (2006). Global temperature calibration of the alkenone unsaturation index ($U^{K'}_{37}$) in surface waters and comparison with surface sediments. *Geochemistry Geophysics Geosystems*, *7*(2).

Coplen, T. B., Brand, W. A., Gehre, M., Gröning, M., Meijer, H. A. J., Toman, B., Verkouteren, R. M. (2006): New Guidelines for ^{13}C Measurements. Analytical Chemistry, 78 (7), 2439-2441.

Corliss, B. H., & Chen, C. (1988). Morphotype patterns of Norwegian Sea deep-sea benthic foraminifera and ecological implications. *Geology*, *16*, 716-719.

den Dulk, M. (1998). Benthic foraminiferal response to variations in surface water productivity and oxygenation in the northern Arabian Sea. *Marine Micropaleontology*, *35*(1-2), 43-66.

den dulk, M., Reichart, G., Vanheyst, S., Zachariasse, W., & Vanderzwaan, G. (2000). Benthic foraminifera as proxies of organic matter flux and bottom water oxygenation? A case history from the northern Arabian Sea. *Palaeogeography, Palaeoclimatology,*

Palaeoecology, *161*(3-4), 337-359.

Gooday, a. J., Levin, L. a., Aranda da Silva, a., Bett, B. J., Cowie, G. L., Dissard, D., Gage, J. D., et al. (2009). Faunal responses to oxygen gradients on the Pakistan margin: A comparison of foraminiferans, macrofauna and megafauna. *Deep Sea Research Part II: Topical Studies in Oceanography*, *56*(6-7), 488-502. Elsevier.

Gooday, A. J., Bernhard, J. M., Levin, L. A., & Suhr, S. B. (2000). Foraminifera in the Arabian Sea oxygen minimum zone and other oxygen-de " cient settings : taxonomic composition , diversity , and relation to metazoan faunas. *Deep-Sea Research*, *47*, 25-54.

Gooday, A. J., Bett, B. J., Shires, R., & Lambshead, P. J. D. (1998). Deep-sea benthic foraminiferal species diversity in the NE Atlantic and NW Arabian sea: a synthesis. *Deep Sea Research Part II: Topical Studies in Oceanography*, *45*(1-3), 165-201.

Hammer, O., Harper, D., (2006): Paleontological Data Analysis,

Harvey, G. . (1980). A study of the chemistry of iodine and bromine ni marine sediments. *Marine Chemistry*, *8*, 327-332.

Hemming, S. R. (2004). Heinrich events: massive Late Pleistocene detritus layers of the North Atlantic and their global climate imprint. *Review of Geophysics*, *31*(2003), 1-43.

Hermelin, J. O. R. (1992). Variations in the benthic foraminiferal fauna of the Arabian Sea: a response to changes in upwelling intensity? *Geological Society, London, Special Publications*, *64*(1), 151-166.

Hermelin, J.O.R., & Shimmield, G. B. (1990). The Importance of the Oxygen Minimum Zone and Sediment Geochemistry in the Distribution of Recent Benthic Foraminifera in the Northwest Indian Ocean. *Geology*, *91*, 1-29.

Hughes, D. J., Lamont, P. A., Levin, L. A., Packer, M., Feeley, K., & Gage, J. D. (2009). Deep-Sea Research II Macrofaunal communities and sediment structure across the Pakistan margin Oxygen Minimum Zone , North-East Arabian Sea. *Deep-Sea Research Part II*, *56*(6-7), 434-448. Elsevier.

Ivanova, E., Schiebel, R., Singh, a, Schmiedl, G., Niebler, H., & Hemleben, C. (2003). Primary production in the Arabian Sea during the last 135000 years. *Palaeogeography, Palaeoclimatology, Palaeoecology*, *197*(1-2), 61-82.

Jan, G., & Tjallingii, R. (2008). Calibration of XRF core scanners for quantitative geochemical logging of sediment cores : Theory and application. *Earth and Planetary Science Letters*, *274*, 423-438.

Jannink, N. T., Zachariasse, W. J., & Van der Zwaan, G. J. (1998). Living (Rose Bengal stained) benthic foraminifera from the Pakistan continental margin (northern Arabian Sea). *Deep Sea Research Part I: Oceanographic Research Papers*, *45*(9), 1483-1513.

Jayaraju, N., Chinnapolla, B., Raja, S., & Reddy, K. R. (2010). Deep-Sea Benthic Foraminiferal Distribution in South West Indian Ocean : Implications to Paleoecology. *International Journal of Geosciences*, *2010*(August), 79-86.

Jorissen, F.J., Wittling, I., Peypouquet, J. P., Rabouille, C., & Relexans, J. C. (1998). Live benthic foraminiferal faunas off Cape Blanc, NW-Africa: Community structure and microhabitats. *Deep Sea Research Part I: Oceanographic Research Papers*, *45*(12), 2157-2188.

Jorissen, Frans J, Fontanier, C., & Thomas, E. (2007). *Paleoceanographical proxies based on deep-sea benthic foraminiferal assemblage characteristics* (Vol. 1, pp. 1-90).

Jorissen, Frans J., de Stigter, H. C., & Widmark, J. G. V. (1995). A conceptual model explaining benthic foraminiferal microhabitats. *Marine Micropaleontology*, *26*(1-4), 3-15.

Kitazato, H. (1994). Foraminiferal microhabitats in four marine environments around Japan. *Marine Micropaleontology*, *24*(1), 29-41.

Klöcker, R., & Henrich, R. (2006). Recent and Late Quaternary pteropod preservation on the Pakistan shelf and continental slope. *Marine Geology*, *231*(1-4), 103-111.

Lisiecki, L. E., Raymo, M. E., & Curry, W. B. (2008). Atlantic overturning responses to Late Pleistocene climate forcings. *Nature*, *456*(7218), 85-8.

Liu, X., & Shi, Z. (2009). Effect of precession on the Asian summer monsoon evolution: A systematic review. *Chinese Science Bulletin*, *54*(20), 3720-3730.

Mayer, L. M., Schick, L. L., Allison, M. a., Ruttenberg, K. C., & Bentley, S. J. (2007). Marine vs. terrigenous organic matter in Louisiana coastal sediments: The uses of bromine:organic carbon ratios. *Marine Chemistry*, *107*(2), 244-254.

Mazumder, A., Henriques, P. J., Nigam, R., & Paula, D. (2003). Distribution of Benthic Foraminifera within Oxygen Minima Zone , off Central West Coast , India.

Paulmier, a., & Ruiz-Pino, D. (2009). Oxygen minimum zones (OMZs) in the modern ocean. *Progress In Oceanography*, *80*(3-4), 113-128. Elsevier Ltd.

Pichevin, L., Bard, E., Martinez, P., & Billy, I. (2007). Evidence of ventilation changes in the Arabian Sea during the late Quaternary: Implication for denitrification and nitrous oxide emission. *Global Biogeochemical Cycles*, *21*(4), 1-12.

Poulton, A.J., A. J., Charalampopoulou, A., Young, J. R., Tarran, G. A., Lucas, M. I. & Quartly, G. D. Coccolithophore dynamics in non-bloom conditions during late summer in the central Iceland Basin (July–August 2007). Limnol. Oceanogr., 55(4), 1601-1613 (2010).

Qasim, S. Z. (1982). Oceanography of the northern Arabian Sea. *Deep-Sea Research*, *29*(9), 1041-1068.

Rad, U Von, & Schulz, H. (1995). Sampling the oxygen minimum zone off Pakistan : glacial-interglacial variations of anoxia and productivity (preliminary results , SoNm 90 cruise). *Marine Geology*, *125*, 7-19.

Rad, Ulrich Von, Schulz, H., Riech, V., Dulk, M. D., Berner, U., & Sirocko, F. (1999). Multiple monsoon-controlled breakdown of oxygen-minimum conditions during the past 30 , 000 years documented in laminated sediments off Pakistan. *Palaeogeography, Palaeoclimatology, Palaeoecology*, *152*, 129-161.

Rai, A. K., & Das, S. S. (2011). Late Quaternary changes in

surface productivity and oxygen minimum zone (OMZ) in the northwestern Arabian Sea : Micropaleontologic and sedimentary record at ODP site 728A. *Earth*, (1), 113-121.

Rai, A. K., & Srinivasan, M. S. (2000). Deep sea benthic foraminiferal response to the pliocene palaeoenvironments of the northen Indian Ocean. *Geobios*, *33*(3), 301-308.

Reichart, G., Dendulk, M., Visser, H., Vanderweijden, C., & Zachariasse, W. (1997). A 225 kyr record of dust supply, paleoproductivity and the oxygen minimum zone from the Murray Ridge (northern Arabian Sea). *Palaeogeography, Palaeoclimatology, Palaeoecology*, *134*(1-4), 149-169.

Reichart, G J, Lourens, L. J., & Zachariasse, W. J. (1998). Temporal variability in the northern Arabian Sea Oxygen Minimum Zone (OMZ) during the last 225 , 000 years. *Paleoceanography*, *13*(6), 607-621.

Reichart, G. J., Nortier, J., Versteegh, G., & Zachariasse, W. J. (2002). Periodical breakdown of the Arabian Sea oxygen minimum zone caused by deep convective mixing. *Geological Society, London, Special Publications*, *195*(1), 407-419.

Reichart, G.-J. (2004). Hyperstratification following glacial overturning events in the northern Arabian Sea. *Paleoceanography*, *19*(2), 1-8.

Reichart, G.J., Schenau, S. J., de Lange, G. J., & Zachariasse, W. J. (2002). Synchroneity of oxygen minimum zone intensity on the Oman and Pakistan Margins at sub-Milankovitch time scales. *Marine Geology*, *185*(3-4), 403-415.

Roche, D., Paillard, D., & Cortijo, E. (2004). Constraints on the duration and freshwater release of Heinrich event 4 through isotope modelling. *Letters to Nature*, *432*, 379-382..

Rostek, F., Bard, E., Beaufort, L. U. C., Sonzogni, C., & Ganssent, G. (1997). Sea surface temperature and productivity records for the past 240 kyr in the Arabian Sea. *Deep-Sea Research II*, *44*, 1461-1480.

Ruddiman, W. F. (2006). What is the timing of orbital-scale monsoon changes? *Quaternary Science Reviews*, *25*(7-8), 657-658.

Ruddiman, W.F. (2008), Earth's climate: past and future, W.H Freeman and Co., NY

Schenau, S.J, Slomp, C. ., & De Lange, G. . (2000). Phosphogenesis and active phosphorite formation in sediments from the Arabian Sea oxygen minimum zone. *Marine Geology*, *169*(1-2), 1-20.

Schenau, S. J. (2002). Oxygen minimum zone controlled Mn redistribution in Arabian Sea sediments during the late Quaternary. *Paleoceanography*, *17*(4).

Schenau, S.J., Passier, H. F., Reichart, G. J., & de Lange, G. J. (2002). Sedimentary pyrite formation in the Arabian Sea. *Marine Geology*, *185*(3-4), 393-402.

Schmiedl, G. (2005). Oxygenation changes in the deep western Arabian Sea during the last 190,000 years: Productivity versus deepwater circulation. *Paleoceanography*, *20*(2), 1-14.

Schmittner, A., Galbraith, E. D., Hostetler, S. W., Pedersen, T. F., & Zhang, R. (2007). Large fluctuations of dissolved oxygen in the Indian and Pacific oceans during Dansgaard-Oeschger oscillations caused by variations of North Atlantic Deep Water subduction. *Paleoceanography*, *22*(3), 1-17.

Schulte, S., Rostek, F., & Bard, E. (1999a). Variations of oxygen-minimum and primary productivity recorded in sediments of the Arabian Sea. *Earth and Planetary Science Letters*, *173*, 205-221.

Schulte, S., Rostek, F., & Bard, E. (1999b). Variations of oxygen-minimum and primary productivity recorded in sediments of the Arabian Sea. *Earth and Planetary Science Letters*, *173*, 205-221.

Schulte, S., Rostek, F., & Bard, E. (1999c). Variations of oxygen-minimum and primary productivity recorded in sediments of the Arabian Sea. *Earth and Planetary Science Letters*, *173*, 205-221.

Schulz, H. (1998). Correlation between Arabian Sea and Greenland climate oscillations of the past 110,000 years. *Letters to Nature*, *393*(May), 23-25.

Schumacher, S., Jorissen, F. J., Dissard, D., Larkin, K. E., & Gooday, A. J. (2007). Live (Rose Bengal stained) and dead benthic foraminifera from the oxygen minimum zone of the Pakistan continental margin (Arabian Sea). *Marine Micropaleontology*, *62*(1), 45-73.

Schumacher, S., Jorissen, F. J., Mackensen, A., Gooday, A. J., & Pays, O. (2010). Ontogenetic effects on stable carbon and oxygen isotopes in tests of live (Rose Bengal stained) benthic foraminifera from the Pakistan continental margin. *Marine Micropaleontology*, *76*(3-4), 92-103. Elsevier B.V.

Section, L. (1993). New evidence for enhanced preservation of organic carbon in contact with oxygen minimum zone on the western continental slope of India. *Science*, *111*, 7-13.

Shackleton, N. J., Vincent, E., Jolla, L., & Calif, U. S. A. (1978). FROM THE Sub-department of Quaternary Research , University of Cambridge , Cambridge (England) more problems than it solves , we hope that at least we draw attention to some fruitful lines of investigation in addition to casting doubt on some previous a. *Marine Micropaleontology*, *3*, 1-13.

Shailaja, M. S., Narvekar, P. V., Alagarsamy, R., & Naqvi, S. W. a. (2006). Nitrogen transformations as inferred from the activities of key enzymes in the Arabian Sea oxygen minimum zone. *Deep Sea Research Part I: Oceanographic Research Papers*, *53*(6), 960-970.

Shimmield, G. B., & Mowbray, S. R. (1991). 23 . The inorganic geochemical record of the northwest Arabian Sea: a history of productivity variations over the last 400 ka. *Proceedings of the Ocean Drilling Program, Scientific Results*, *117*.

Sikes, E. L., Keigwin, L. D., & Farrington, J. W. (1991). Use of the alkenone unsaturation ratio U3 k to determine past sea surface temperatures " core-top SST calibrations and methodology considerations. *Planetary Sciences*, *104*, 36-47.

Singh, A D. (2007). Episodic preservation of pteropods in the eastern Arabian Sea : Monsoonal change , oxygen minimum zone intensity and aragonite compensation depth. *Indian Journal of Marine Sciences*, *36*(December), 378-383.

Singh, Arun Deo, Jung, S. J. a., Darling, K., Ganeshram, R., Ivanochko, T., & Kroon, D. (2011). Productivity collapses in the Arabian Sea during glacial cold phases. *Paleoceanography*, *26*(3), PA3210.

Sirocki, F., Sarnthein, M., Erlenkeuser, H., Lange, H., M., A., & Duplessy, J. C. (1993). Century-scale events in monsoonal climate over the past 24,000 years. *Letters to Nature*, *364*.

Sonzogni, C., Bard, E., Rostek, F., Lafont, R., & Rosell-melets, A. (1997). Core-top calibration of the alkenone index vs sea surface temperature in the Indian Ocean. *Deep-Sea Research Part II*, *44*(6), 1445-1460.

Staubwasser, M., & Dulski, P. (2002a). On the evolution of the oxygen minimum zone in the Arabian Sea during Holocene time and its relation to the South Asian monsoon. *Geological Society, London, Special Publications*, *195*(1), 433-443.

Staubwasser, M., & Dulski, P. (2002b). On the evolution of the oxygen minimum zone in the Arabian Sea during Holocene time and its relation to the South Asian monsoon. *Geological Society, London, Special Publications*, *195*(1), 433-443.

Stramma, L., Johnson, G. C., Sprintall, J., & Mohrholz, V. (2008). Expanding oxygen-minimum zones in the tropical oceans. *Science (New York, N.Y.)*, *320*(5876), 655-8.

Stramma, L., Prince, E. D., Schmidtko, S., Luo, J., Hoolihan, J. P., Visbeck, M., Wallace, D. W. R., et al. (2011). Expansion of oxygen minimum zones may reduce available habitat for tropical pelagic fishes. *Nature Climate Change*, *2*(1), 33-37. Nature Publishing Group.

Stramma, L., Schmidtko, S., Levin, L. a., & Johnson, G. C. (2010). Ocean oxygen minima expansions and their biological impacts. *Deep Sea Research Part I: Oceanographic Research Papers*, *57*(4), 587-595. Elsevier.

Sun, Y., Wu, F., Clemens, S. C., & Oppo, D. W. (2008). Processes controlling the geochemical composition of the South China Sea sediments during the last climatic cycle. *Chemical Geology*, *257*(3-4), 240-246. Elsevier B.V.

Tjallingii, R., Ro, U., & Ko, M. (2007). scanning measurements in soft marine sediments. *Geochemistry Geophysics Geosystems*, (13), 1-12.

Tribovillard, N., Algeo, T. J., Lyons, T., & Riboulleau, A. (2006). Trace metals as paleoredox and paleoproductivity proxies: An update. *Chemical Geology*, *232*(1-2), 12-32.

Villanueva, J., Pelejero, C., & Grimalt, J. O. (1997). Clean-up procedures for the unbiased estimation of C37 alkenone sea surface temperatures and terrigenous n-alkane inputs in paleoceanography. *Journal of Chromatography A*, *757*(1-2), 145-151.

von Rad, U., Schaaf, M., Michels, K. H., Schulz, H., Berger, W. H., & Sirocko, F. (1999). A 5000-yr Record of Climate Change in Varved Sediments from the Oxygen Minimum Zone off Pakistan, Northeastern Arabian Sea. *Quaternary Research*, *51*(1), 39-53.

von Rad, U., Schaaf, M., Michels, K. H., Schulz, H., Berger, W. H., & Sirocko, F. (1999). A 5000-yr Record of Climate Change in Varved Sediments from the Oxygen Minimum Zone off Pakistan, Northeastern Arabian Sea. *Quaternary Research*, *51*(1), 39-53.

Wakeham, P. and. (1987). Calibration of unsaturation patterns in long-chain ketone copositions for paleotemperature assessment. *Nature*.

Wang, P., Clemens, S., Beaufort, L., Braconnot, P., Ganssen, G., Jian, Z., Kershaw, P., et al. (2005). Evolution and variability of the Asian monsoon system: state of the art and outstanding issues. *Quaternary Science Reviews*, *24*(5-6), 595-629.

Wang, Y., Cheng, H., Edwards, R. L., Kong, X., Shao, X., Chen, S., Wu, J., et al. (2008). Millennial- and orbital-scale changes in the East Asian monsoon over the past 224,000 years. *Nature*, *451*(7182), 1090-3.

Wehausen, R. (2002). Astronomical forcing of the East Asian monsoon mirrored by the composition of Pliocene South China Sea sediments. *Earth and Planetary Science Letters*, *201*, 621-636.

Wei, G., Liu, Y., Li, X., Shao, L., & Liang, X. (2003). Climatic impact on Al, K, Sc and Ti in marine sediments: Evidence from ODP Site 1144, South China Sea. *Geochemical Journal*, *37*(5), 593-602.

Ziegler, M., Lourens, L. J., Tuenter, E., & Reichart, G.-J. (2010). High Arabian Sea productivity conditions during MIS 13 – odd monsoon event or intensified overturning circulation at the end of the Mid-Pleistocene transition? *Climate of the Past*, *6*(1), 63-76.

Ziegler, M., Tuenter, E., & Lourens, L. J. (2010b). The precession phase of the boreal summer monsoon as viewed from the eastern Mediterranean (ODP Site 968). *Quaternary Science Reviews*, *29*(11-12), 1481-1490. Elsevier Ltd.

Ziegler, Martin, Jilbert, T., de Lange, G. J., Lourens, L. J., & Reichart, G.-J. (2008). Bromine counts from XRF scanning as an estimate of the marine organic carbon content of sediment cores. *Geochemistry Geophysics Geosystems*, *9*(5), 1-6.

Ziegler, Martin, Lourens, L. J., Tuenter, E., Hilgen, F., Reichart, G. J., & Weber, N. (2010). Precession phasing offset between Indian summer monsoon and Arabian Sea productivity linked to changes in Atlantic overturning circulation. *Hemisphere*, *25*, 1-16.

Ziegler, Martin, Lourens, L. J., Tuenter, E., Hilgen, F., Reichart, G.-J., & Weber, N. (2010a). Precession phasing offset between Indian summer monsoon and Arabian Sea productivity linked to changes in Atlantic overturning circulation. *Paleoceanography*, *25*(3), 1-16.

Ziegler, Martin, Nürnberg, D., Karas, C., Tiedemann, R., & Lourens, L. J. (2008). Persistent summer expansion of the Atlantic Warm Pool during glacial abrupt cold events. *Nature Geoscience*, *1*(9), 601-605.

van der Weijden, C. H., Reichart, G. J., & Visser, H. J. (1999). Enhanced preservation of organic matter in sediments deposited within the oxygen minimum zone in the northeastern Arabian Sea. *Deep Sea Research Part I: Oceanographic Research Papers*, *46*(5), 807-830.

van der Weijden, C. H., Reichart, G.-J., & van Os, B. J. H. (2006). Sedimentary trace element records over the last 200 kyr from within and below the northern Arabian Sea oxygen minimum zone. *Marine Geology*, *231*(1-4), 69-88.